LSA SAF Meteosat FRP Products: Part 2 - Evaluation and demonstration for use in the Copernicus Atmosphere Monitoring Service (CAMS)

Roberts, G[1]*., Wooster, M. J[23]., Xu, W[2]., Freeborn, P. H[6]., Morcrette, J-J[5]., Jones, L[5], Benedetti, A[5], Jiangping, H[2]., Fisher, D[2]. and Kaiser, J. W[4]

*corresponding author

1) Geography and Environment, University of Southampton, Southampton, UK
2) Department of Geography, Kings College London, London, UK
3) NERC National Centre for Earth Observation, Leicester, UK
4) Max Planck Institute for Chemistry, Mainz, Germany
5) European Center for Medium-Range Weather Forecasts, Reading, UK
6) Fire Sciences Laboratory, Missoula, USA

ABSTRACT

Characterising the dynamics of landscape scale wildfires at very high temporal resolutions is best achieved using observations from Earth Observation (EO) sensors mounted onboard geostationary satellites. As a result, a number of operational active fire products have been developed from the data of such sensors. An example of which are the Fire Radiative Power (FRP) products, the FRP-PIXEL and FRP-GRID products, generated by the Land Surface Analysis Satellite Applications Facility (LSA SAF) from imagery collected by the Spinning Enhanced Visible and Infrared Imager (SEVIRI) on-board the Meteosat Second Generation (MSG) series of geostationary EO satellites. The processing chain developed to deliver these FRP products detects SEVIRI pixels containing actively burning fires and characterises their FRP output across four geographic regions covering Europe, part of South America and northern and southern Africa. The FRP-PIXEL product contains the highest spatial and temporal resolution FRP dataset, whilst the FRP-GRID product contains a spatio-temporal summary that includes bias adjustments for cloud cover and the non-detection of low FRP

fire pixels. Here we evaluate these two products against active fire data collected by the Moderate Resolution Imaging Spectroradiometer (MODIS), and compare the results to those for three alternative active fire products derived from SEVIRI imagery. The FRP-PIXEL product is shown to detect a substantially greater number of active fire pixels than do alternative SEVIRI-based products, and comparison to MODIS on a per-fire basis indicates a strong agreement and low bias in terms of FRP values. However, low FRP fire pixels remain undetected by SEVIRI, with errors of active fire pixel detection commission and omission compared to MODIS ranging between 9 - 13% and 65 - 77% respectively in Africa. Higher errors of omission result in greater underestimation of regional FRP totals relative to those derived from simultaneously collected MODIS data, ranging from 35% over the Northern Africa region to 89% over the European region. High errors of active fire omission and FRP underestimation are found over Europe and South America, and result from SEVIRI's larger pixel area over these regions. An advantage of using FRP for characterising wildfire emissions is the ability to do so very frequently and in near real time (NRT). To illustrate the potential of this approach, wildfire fuel consumption rates derived from the SEVIRI FRP-PIXEL product are used to characterise smoke emissions of the 2007 'mega fire' event focused on Peloponnese (Greece) and used within the European Centre for Medium-Range Weather Forecasting (ECMWF) Integrated Forecasting System (IFS) as a demonstration of what can be achieved when using geostationary active fire data within the Copernicus Atmosphere Monitoring Service (CAMS). Qualitative comparison of the modelled smoke plumes with MODIS optical imagery illustrates that the model captures the temporal and spatial dynamics of the plume very well, and that high temporal resolution emissions estimates such as those available from geostationary orbit are important for capturing the sub-daily variability in smoke plume parameters such as aerosol optical depth (AOD), which are increasingly less well resolved using daily or coarser temporal resolution emissions datasets. Quantitative comparison of modelled AOD with coincident MODIS and AERONET AOD indicates that the former is overestimated by ~20 - 30%, but captures the observed AOD dynamics with a high degree of fidelity. The case study highlights the potential of using geostationary FRP data to drive fire emissions estimates for use within atmospheric transport models such as those implemented in the Monitoring Atmospheric Composition and Climate (MACC) series of projects for the CAMS.

1. INTRODUCTION

1.1. Biomass Burning Emissions and Meteosat SEVIRI FRP Products from the LSA SAF

Biomass burning emissions databases derived from Earth Observation (EO) satellite data, such as the widely used Global Fire Emissions Database (GFED; van der Werf *et al.,* 2006; 2010), typically follow the approach proposed by Seiler and Crutzen (1980) and estimate fire emissions via the multiplication of burned area (m^2), fuel load (kg m^{-2}) and combustion completeness (unitless, 0-1) estimates. Emissions databases developed in this manner have been widely applied to deliver wildfire emissions of trace gases and aerosols for use in atmospheric transport models (Mu *et al.,* 2011; Tsyro *et al.,* 2007). However, whilst excellent for many applications, some limitations of this 'burned area' based approach are that it works only after the fire event, cannot be applied in near real-time, and has a relatively low temporal resolution that provides little or no information on the variability of the emissions during the fire itself. All these maybe limitations when modelling certain aspects of fire emissions transport and generally preclude use of the approach in real-time atmospheric monitoring or forecasting systems (Reid *et al.*, 2004). The companion paper to this work, Wooster *et al.* (2015) describes the geostationary Meteosat SEVIRI Fire Radiative Power (FRP) products being generated operationally by the EUMETSAT Land Surface Analysis Satellite Applications Facility (LSA SAF; http://landsaf.meteo.pt/). This type of geostationary active fire product offers an alternative route to biomass burning emissions estimation based on assessments of the thermal energy being radiated away from fires, and can do so in near real-time with frequent updates whilst the fires are still burning, though there are also some limitations caused mainly by fires having too low a fire radiative power remaining undetectable with the relatively coarse spatial resolution SEVIRI observations (Roberts and Wooster, 2008). Whilst Wooster *et al.* (2015) describe the methodologies and algorithms used to produce the LSA SAF Meteosat FRP products, and their information characteristics, the purpose of the current work is to (i) provide a full evaluation of the product compared to other real-time active fire products derived from the same SEVIRI observations, (ii) to provide a product validation via comparisons to the widely used and higher spatial resolution (albeit lower temporal resolution) MODIS active fire detections, and (iii) to demonstrate how the product can be used as a high temporal resolution biomass burning emissions driver

within a case study that exploits components of the prototype CAMS (http://www.copernicus-atmosphere.eu/)

1.2. Satellite Earth Observation Active Fire Products

Active fire products that are based on detecting the thermal radiation being emitted by landscape scale fires have been available for over three decades from numerous polar orbiting and geostationary satellites (Prins *et al.*, 1994; Prins *et al.*, 1998; Matson, 1981, Justice *et al.*, 1998; Giglio, 2003b). In addition to simple detection, Dozier (1981) first demonstrated the additional potential to estimate a fire's subpixel effective temperature and fractional area, and this approach has been applied in the Wildfire Automated Biomass Burning Algorithm (WFABBA) to data from the Geostationary Operational Environmental Satellite (GOES) for over two decades (Prins *et al.*, 1994). Building on this idea, the FRP route to characterising active fires and estimate wildfire emissions was first proposed by Kaufman *et al.* (1996). The FRP approach is based on the understanding that the amount of heat produced by burning a fixed mass of biomass is relatively invariant to vegetation type (Jenkins *et al.*, 1998). By measuring the component of this "heat of combustion" that is radiated away from the surface, the amount of vegetation being burned per second can then be estimated (Wooster *et al.*, 2003; Wooster *et al.*, 2005; Freeborn *et al.*, 2008). An advantage of the FRP approach for estimating smoke emissions to the atmosphere is that it is based on a direct remotely sensed observation, and a large number of polar and geostationary satellite instruments have the requisite midwave infrared (MWIR) waveband required to estimate FRP using the MIR radiance approach of Wooster *et al.* (2003; 2005). The Moderate Resolution Imaging Spectroradiometer (MODIS) instruments onboard the Terra and Aqua satellites have been providing FRP measurements since 2000 and 2002 respectively (Kaufman *et al.*, 1998; Giglio *et al.*, 2003b) and is currently supported by the Visible Infrared Imaging Radiometer Suite (VIIRS) onboard Suomi-NPP (Csiszar *et al.*, 2014) and the soon-to-be-launched Sea and Land Surface Temperature Radiometer (SLSTR) onboard Sentinel-3 (Wooster *et al.*, 2012). Geostationary instruments, such as the Geostationary Operational Environmental Satellite (GOES) imager (Xu *et al.*, 2010), are also providing FRP measurements at much higher temporal resolution but at lower spatial resolution and coverage, and those from the Meteosat SEVIRI instrument (Wooster *et al.*, 2015) are the target of the current work.

1.3. Wildfire Emissions Datasets from FRP Observations

Information on the fuel consumption totals required to build wildfire emissions inventories have already been developed using FRP data derived from polar-orbiter (Vermote *et al.*, 2009; Ellicott *et al.*, 2009; Kaiser *et al.*, 2012) and geostationary satellite EO data (Pereira *et al.*, 2011; Roberts *et al.*, 2011). A limitation associated with the former is their intermittent observation of the diurnal fire cycle, which needs to be characterised in order to estimate daily Fire Radiative Energy (FRE; the temporal integration of FRP). MODIS typically provides around four daily observations depending on latitude which, when accumulated over a sufficiently long time period, have been exploited to model the diurnal fire cycle and estimate total emissions over 8-day or longer periods (Vermote *et al.*, 2009; Ellicott *et al*, 2009). Geostationary FRP datasets provide much higher observation frequencies, and thus unparalleled data on the diurnal fire cycle (e.g. Roberts and Wooster, 2007; Roberts *et al.*, 2009;), and Zhang *et al.* (2012) illustrate one way such data can be used to develop a near global biomass burning emissions dataset at hourly type temporal resolutions. However, a limitation of geostationary data is their coarse spatial resolution, which results biases in regional-scale FRP and FRE due to the omission of small and/or low intensity wildfires (Roberts *et al.*, 2005; Xu *et al.*, 2010). Freeborn *et al.* (2009) addressed this issue by synthesising a 'virtual' FRP product via the integration of both geostationary and polar-orbiter FRP data, maintaining the high temporal resolution of geostationary data whilst simultaneously adjusting them for the active fire detection biases using the higher spatial resolution MODIS measurements. Roberts *et al.* (2011) blended geostationary FRP data with MODIS-derived burned area information to meet a similar objective.

Perhaps the most obvious advantage FRP-based biomass burning emissions inventories offer over a burned area based inventory is their near real-time capability, since the thermal radiation being emitted by the active fires is being sensed whilst the fire is actually burning, rather than somewhat after the event. As a result, FRP-derived emissions estimates are being increasing applied to characterise wildfire emissions for use in near real time atmospheric transport models. Sofiev *et al.* (2009) use MODIS FRP measurements to characterise particulate matter (PM) emissions using the method proposed by Ichoku and Kaufmann (2005), and the dispersion of the resulting emissions are propagated using the System for Integrated modeLling of Atmospheric coMposition (SILAM) dispersion model. In this approach, the diurnal variation of emissions is specified as being 25% greater than the daily mean during the day, and 25% less than the mean during the night. Kaiser *et al.* (2009a; 2012) developed the Global Fire Assimilation System (GFAS) to prescribe wildfire emissions

for use in the CAMS, potentially calculating the FRP density emitted by actively burning fires (mW m^{-2}) using a variety of FRP measurements from different spacecraft. However, in the NRT version of GFAS used currently only FRP measurements from MODIS are used. The FRE density (J m^{-2}) is estimated by temporally integrating the MODIS-derived FRP density using a Kalman filter. Most recently, Turquety *et al.* (2014) used SEVIRI FRP measurements from the LSA SAF products to prescribe the fire diurnal cycle for the APIFLAME European fire emissions model, and Baldassarre *et al.* (2015) used both the LSA SAF SEVIRI FRP products and other active fire products to simulate the emissions and emissions transport of a large fire in Turkey.

This manuscript provides a detailed evaluation of the Meteosat SEVIRI FRP products available from the LSA SAF, both the full resolution FRP-PIXEL product and the reduced resolution FRP-GRID product, both available in near real time and in archived form (http://landsaf.meteo.pt/), and provides a detailed example of their use in characterising wildfire emissions and its atmospheric transport at high temporal resolution. Section 2 provides a brief product summary, and readers are referred to the companion paper (Wooster *et al.*, 2015) for a more detailed description of the algorithms used to derive the information from the raw SEVIRI level 1.5 observations. Sections 3 describes a detailed inter-comparison of the LSA SAF SEVIRI FRP-PIXEL product with both the MODIS active fire products (Giglio *et al.,* 2003), and three alternative active fire products also derived from SEVIRI observations: namely the WFABBA (Prins *et al.,* 1998), Fire Detection and Monitoring (FDeM; Amraoui *et al.,* 2010) and Active Fire Monitoring (FIR) product (Joro *et al.,* 2008). Section 4 evaluates the specific performance of spatio-temporal summary 'FRP-GRID' product available from the LSA SAF, which incorporates statistical adjustments for SEVIRI's regional FRP biases, whilst Section 5 describes use of the FRP-PIXEL product for parameterising wildfire emissions at high temporal resolution within the ECMWF Integrated Forecasting System (IFS) atmospheric chemistry and transport model that is used to deliver the CAMS (http://www.copernicus-atmosphere.eu/).

2. METEOSAT SEVIRI FRP PRODUCTS FROM THE EUMETSAT LSA SAF

The Spinning Enhanced Visible and Infrared Imager (SEVIRI) onboard the Meteosat Second Generation (MSG) series of satellites acquires observations every 15 minutes over the Earth's disk centred on West Africa, including in MWIR and long-wave infrared (LWIR) wavebands.

Data collected in these wavebands enables the detection of active fires using the type of algorithms detailed in Li *et al.* (2001), and this has been exploited for the development of a number of geostationary active fire products based on SEVIRI observations. One of these is the Meteosat SEVIRI FRP-PIXEL family of products that has been produced operationally since 2008 by the European Organisation for the Exploitation of Meteorological Satellites (EUMETSAT) LSA SAF (http://landsaf.meteo.pt). The LSA SAF Meteosat SEVIRI FRP product suite currently contains two components; (i) the FRP-PIXEL product which records active fire information at the full temporal and spatial resolution of SEVIRI, and (ii) the FRP-GRID product that provides a spatio-temporal summary of the FRP-PIXEL product, along with statistical adjustments for cloud cover and for the regional biases caused by the lowest FRP fires being undetectable with SEVIRI.

2.1 FRP-PIXEL Product Summary

The Level 2 FRP-PIXEL product provides information on the spatial location, thermal properties, atmospherically corrected FRP and uncertainty of pixels containing actively burning fires every 15 minutes over Europe, North and South Africa and part of South America (Figure 1), based upon an extended version of the geostationary Fire Thermal Anomaly (FTA) active fire detection algorithm of Roberts and Wooster (2008) and a set of FRP estimation routines that are together fully detailed in Wooster *et al.* (2015). The structure of the FRP-PIXEL product is also detailed in Wooster *et al.* (2015), and follows the heritage of the MODIS active fire products (Giglio *et al.*, 2003) but separated into two discrete files, (i) the FRP-PIXEL 'Quality Product' file, a 2D dataset that provides information on the status of each SEVIRI pixel in the geographic region under study (e.g. whether it is a cloud, water, or land pixel, whether it has been classed as containing an active fire etc; Wooster *et al.*, 2015), and (ii) a smaller 'List Product' file that provides detailed information of pixels in which active fires have been detected (e.g. including the pixel MWIR and LWIR brightness temperatures, FRP, FRP uncertainty, latitude and longitude, and some of the metrics derived during algorithm application such as background window size and estimated MWIR band atmospheric transmissivity).

2.2 FRP-GRID Product Summary

The Level 3 FRP-GRID product is a spatio-temporal summary of a series of FRP-PIXEL products. At the regional scale, the FRP-PIXEL product provides a minimum estimate of the FRP being emitted from landscape fires due to (i) the inability of SEVIRI to detect the lowest FRP active fire pixels (Roberts and Wooster, 2008; Freeborn *et al.*, 2014a) and (ii) the fact that the assessment of the highest FRP fires suffer from some effects of pixel saturation and other SEVIRI-specific observation characteristics (Wooster *et al.*, 2015). In order to try mitigate these impacts on regional FRP estimation, the LSA SAF processing chain generates the Level 3 FRP-GRID product by temporally accumulating active fire pixels and associated information from the maximum of four FRP-PIXEL products obtained each hour, grids this information within 5.0° grid cells, and applies a set of regional bias adjustment factors. Wooster *et al.* (2015) describe the procedures in full, and an evaluation of the resulting product performance is presented in Section 4 herein.

3. FRP-PIXEL PRODUCT PERFORMANCE EVALUATION

Here we validate the SEVIRI FRP products using MODIS active fire data. The relatively high spatial resolution of MODIS' active fire observations (1 km at nadir), and the high saturation temperature of its MWIR channel (~ 500 K), coupled with its better than daily availability from two platforms (the Terra and Aqua satellites), ensure that the MODIS active fire product (Kaufman *et al.*, 1998; Giglio *et al.* 2003) is the standard against which geostationary active fire products are compared when performing product evaluations (Xu *et al.*, 2010; Schroeder *et al.*, 2014; Roberts and Wooster, 2014). Here we use near-simultaneously recorded Collection 5 MODIS active fire detections (MOD14 from Terra and MYD14 from Aqua) as the basis of our LSA SAF SEVIRI FRP Product performance evaluations. For completeness, we also include a series of other SEVIRI active fire products, derived using different algorithms and methods to the LSA SAF FRP products, within the same comparison.

3.1 SEVIRI FRP-PIXEL and MODIS Active Fire Product Intercomparison

3.1.1 Methodology

The FRP-PIXEL product is generated in separate files for the four LSA SAF geographic regions whose boundaries as shown in Figure 1 (Wooster *et al.*, 2015). We conducted the FRP-PIXEL product performance evaluation using one week of operational FRP-PIXEL data collected by Meteosat-9 in each of the LSA SAF regions, together with the matching MODIS MOD14 and MYD14 products. The FRP-PIXEL products of each region were derived from 672 separate SEVIRI imaging slots taken every 15 minutes over a 168 hour period in 2008, with the timing of the products for each geographic region being that corresponding to its peak fire period; December in Northern hemisphere Africa, and August in the remaining three regions. Freeborn *et al.* (2014a) previously performed an evaluation of the FRP-PIXEL product over the Central African Republic (CAR), finding that the products active fire detection errors of commission reduced greatly (from 24% to 9%) when the MODIS active fire detections being used as the independent data source were limited to a ± 18.6° scan angle. This is due to the increasing pixel area of MODIS with increasing scan angle, which results in MODIS itself showing progressively greater active fire errors of omission towards the scan edge (Freeborn *et al.*, 2011). When comparing large-scan angle MODIS data to active fire detections made from SEVIRI, it may well be that MODIS actually misses fires that the SEVIRI FRP-PIXEL product actually correctly detects, but in the absence of any other information a SEVIRI-to-MODIS performance evaluation would record this as a SEVIRI commission error. Therefore, to mitigate against the impact of MODIS' decreasing ability to detect low FRP pixels as MODIS scan angle increases, yet balance this with the need to maintain sufficient data in our intercomparison, MODIS observations are limited to those within ± 30° scan angle within which MODIS' pixel area increases up to a maximum of 1.7 km² from the nadir 1 km² size (Freeborn *et al.*, 2011). For each LSA SAF geographic region we compared the active fire detections made by MODIS within this scan angle limit to the active fire pixels present in the FRP-PIXEL product subsets covering the same area and collected at the closest matching time (generally this will be within ~ 6 minutes of the MODIS overpass). To deal with the differing MODIS and SEVIRI pixel sizes, we remapped the MODIS active fire data to SEVIRI's imaging grid. SEVIRI's per-pixel point spread function (PSF) at the sub-satellite point extends more than 5 km radially from the pixel centre (Wooster *et al.*, 2015), so following the approach of Freeborn *et al.* (2014a) we evaluated active fire detection performance using the presence of an active fire pixel within a 3×3 pixel window centred on the active fire pixel under investigation within this grid as a matched detection. For SEVIRI errors of commission we searched for the presence of a

matching MODIS pixel for each SEVIRI active fire pixel studied, whilst the reverse analysis was conducted for SEVIRI errors of omission.

When undertaking the SEVIRI-to-MODIS FRP intercomparison, this was conducted on a 'per fire' basis by clustering the MODIS and SEVIRI per-pixel FRP measurements for the same fire into ‘fire pixel clusters’ on the basis of spatial closeness (e.g. Zhukov *et al.*, 2006; Roberts and Wooster; 2008; Xu *et al.*, 2010). The MODIS FRP measurements were derived using the same MIR radiance approach to FRP derivation as is used for SEVIRI (Wooster *et al.*, 2005; 2015), and as will be employed in the forthcoming Collection 6 MODIS Active fire products (L. Giglio, *pers comm.*, 2014). We atmospherically corrected these MODIS FRP estimates using the same procedure applied when generating the FRP-PIXEL product, detailed in Wooster *et al.* (2015), based on an atmospheric transmission look-up-table (LUT) developed using the MODTRAN5 and RTMOM atmospheric radiative transfer models (Berk *et al.* 2005; Govaerts, 2006) and ECMWF forecasts of total water column vapour (interpolated from an original spatial and temporal resolution of 0.5° and 3 hours). Generally, the adjustment for the MWIR atmospheric transmission made to the SEVIRI FRP data was larger than that for MODIS, because the SEVIRI MWIR spectral band used in FRP derivation is significantly wider than that of MODIS and extends into spectral regions having much lower atmospheric transmission (Wooster *et al.*, 2015).

3.1.2 Results

The results of our SEVIRI-to-MODIS per-fire active fire detection intercomparison are detailed in Table 1, Columns 3 and 4. Taking the north African (NAfr) LSA SAF region as the first example, this is closest region to the Meteosat sub-satellite point and therefore offers the highest degree of SEVIRI spatial detail and smallest pixel area. We find that 65% of MODIS’ active fire detections made within this region had no corresponding SEVIRI-detected active fire within the closest matching (in time) FRP-PIXEL product file. This 'active fire error of omission' rate is higher than the 54% found previously by Roberts and Wooster (2008) over the same geographic area, but using the prototype SEVIRI FTA algorithm, a different period satellite (Meteosat-8) and different time period. The reverse analysis showed that 9% of the Meteosat-9 FRP-PIXEL product active fire pixels had no matching MODIS active fire pixel, a very similar commission error to that found by Roberts and Wooster (2008) for the prototype SEVIRI FTA algorithm over the same North African region.

SEVIRI FRP-PIXEL product active fire detection performance metrics for the other three LSA SAF geographic regions are also shown in Table 1, and indicate a substantially increased active fire omission error in South America and Europe compared to the two African regions. This is in part due to SEVIRIs increased pixel area and greater view zenith angle (and thus greater atmospheric attenuation) over the former two regions which are further from the Meteosat sub-satellite point (SSP). South America and Europe have a mean view zenith angle of 59° and 54° respectively and this significantly raises the minimum per-pixel FRP detection limit in these areas (Figure 1), meaning a greater proportion of lower FRP landscape-scale fires fail to be detected by SEVIRI in comparison to the African regions.

Figure 2 and Table 1 (Column 5) present the results of the SEVIRI-to-MODIS per-fire FRP intercomparison. Again taking north Africa as an example, on a per-fire basis there is a strong correlation between the FRP measures made by SEVIRI in this region and by MODIS (Figure 2; top left) with over half (53%) of the SEVIRI-to-MODIS matchups having an FRP difference less than 20%. In fact, a strong level of agreement exists for all regions in terms of a low FRP bias between the two datasets, but there is significant scatter. Overall, we find that 57% of the FRP-PIXEL products per-fire FRP measures are within 20% of those of MODIS, and this level of agreement remains consistent even when limiting the comparison to fires with FRP > 50 MW to ensure we focus on the FRP range where SEVIRI does not clearly underdetect active fires (e.g. Wooster *et al.*, 2015). This suggests that the degree of variability seen between the near-simultaneous measures of per-fire FRP provided by SEVIRI and MODIS is not driven only by active fire pixel errors of omission (e.g. by SEVIRI failing to detect some of the low FRP fire pixels making up a fire cluster), but maybe impacted by other aspects of the FRP measurement process coming from:

i) uncertainty in the ambient background signal used to calculate the FRP for each fire pixel with SEVIRI and MODIS data (Wooster *et al.*, 2003; 2005; Zhukov *et al.*, 2006; Wooster *et al.*, 2015);

ii) the ± 6 minute time difference between corresponding MODIS and SEVIRI observations of the same fire, during which changes in the active fire characteristics that determine the fires FRP may occur;

iii) the uncertainties present in the MODIS FRP measures coming from the sub-pixel location of the fire with respect to the sensor instantaneous field of view, recently been characterised by Freeborn *et al.* (2014c), and with SEVIRI also from certain image processing operations conducted during the production of SEVIRI level 1.5 data (Wooster *et al.*, 2015).

iv) effects of sensor saturation of SEVIRI's MWIR channel at high FRP fire pixels.

To place the magnitude of the scatter seen in Figure 2 between the SEVIRI FRP-PIXEL product's FRP measures and those from the MODIS MOD14 and MYD14 products into context, during the recent Freeborn *et al.* (2014c) study, multiple MODIS FRP measurements of the same fires made almost simultaneously (<< 1 sec difference) in consecutive MODIS scans were compared and some large scan-to-scan differences found. An approximately normally distributed percentage difference between the two FRP measures, with a mean close to zero but a standard deviation of 26.6% was determined from a large dataset of such matchups (Freeborn *et al.*; 2014c). Further investigation showed that the scan-to-scan differences were largely controlled by the differing sub-pixel location of the fire within the different MODIS scans, a subject previously indicated as potentially significant with regard to FRP observations made by the BIRD Hot Spot Recognition Sensor (HSRS; Zhukov *et al.*, 2006). Freeborn *et al.* (2014c) also showed that the scatter reduced as fire clusters containing increasing numbers of active fire pixels were compared, since the sub-pixel location effects would increasingly cancel out as more pixels were included in the instantaneous scan-to-scan FRP inter-comparison. Nevertheless, given the degree of scatter found between even almost totally simultaneous MODIS FRP observations of the same fire made at the same scan angle and pixel area by Freeborn *et al.* (2014c), it is unsurprising that higher levels of scatter arises when comparing FRP data from different sensors (Figure 2; Table 1), where pixel areas, scan angles and imaging time differences are all somewhat greater. Nevertheless, our results indicate that when the FRP-PIXEL product and the MODIS active fire products both detect the same fire, the FRP reported by the two products show small biases. Over the four LSA SAF regions, 391 individual active fire 'clusters' detected by MODIS and SEVIRI were compared and 76% (298 fire clusters) had an FRP within 30% of that measured by MODIS. Given the uncertainties on per-fire FRP retrievals, the LSA SAF target accuracy of the FRP-PIXEL product is specified as, on a per-fire basis, 70% of the SEVIRI-retrieved FRP values being within 50% of those simultaneously measured by MODIS. Therefore, the FRP-PIXEL

product significantly exceeds this specification, and actually approaches that specified by the LSA SAF 'optimal accuracy' definition (70% of retrieved SEVIRI-retrieved FRP value being within 20% of the MODIS-derived value on a per-fire basis).

Whilst our per-fire FRP inter-comparison has indicated a comparatively low degree of FRP bias between the FRP-PIXEL and MODIS MOD14/MYD14 FRP records of the same successfully detected active fires, there remains a significant degree of regional-scale FRP underestimation by the FRP-PIXEL product due to the inability of the coarser SEVIRI observations to detect the lowest FRP component of a regions fire regime (Roberts and Wooster, 2008). Therefore when data from both the MOD14/MYD14 and near-simultaneous matching FRP-PIXEL products covering the same area (i.e. the area covered by MODIS within a ±30° scan angle) are compared, SEVIRI reports a lower cumulative 'regional' FRP than does MODIS (Table 1, Column 6). This effect is directly related to SEVIRI's aforementioned active fire errors of omission, an effect that is magnified in geographic regions in which SEVIRI mostly observes at higher view zenith angles. Figure 3 again uses the example of the North African region, where the slope of the linear of best fit to the regional FRP totals recorded near simultaneously in the FRP-PIXEL product and the MODIS active fire products is 0.65. This indicates the relatively small, but certainly not insignificant, impact of the FRP-PIXEL products active fire errors of omission in this region, which is that closest to the Meteosat sub-satellite point (SSP) and thus in which the FRP-PIXEL products active fire errors of omission are lowest (Table 1). Regional FRP underestimation increases away from the SSP, and appears particularly extreme in the European LSA SAF geographic region in our inter-comparison. This is in part a result of a large proportion of active fires being present in Eastern Europe during our inter-comparison period, where the SEVIRI view zenith angle exceeds 60°. With respect to regional FRP characterisation, the performance of the FRP-PIXEL product for southern European fires, which lie relatively close to the Meteosat SSP, is likely to be much closer to that of the North African geographic region. Section 5 includes study of the August 2007 Greek Fires as a case study example of fires in this region.

3.2 Inter-comparison of Alternative SEVIRI Active Fire Products

Since the launch of Meteosat Second Generation in 2002, a number of studies have used different algorithms to study active fires with SEVIRI observations (e.g. Calle *et al.*, 2009; Amraoui *et al.*, 2010). This has led to certain other routinely generated SEVIRI active fire

products being available, in addition to the LSA SAF FRP-PIXEL product focused upon herein. These alternative SEVIRI-based products include the Wildfire Automated Biomass Burning Algorithm (WFABBA, version 6.5) product (based on the WFABBA fire detection algorithm of Prins *et al.,* 1998), the Fire Detection and Monitoring (FDeM) product (Amraoui *et al.,* 2010), and the Active Fire Monitoring (FIR) product (Joro *et al.,* 2008), each of which essentially generate active fire pixel detections from SEVIRI level 1.5 data as does the FTA algorithm used within the FRP-PIXEL product processing chain (Wooster *et al.,* 2015).

3.2.1 Methodology

We assessed the active fire detection performance of the FRP-PIXEL product in comparison to the three main alternative SEVIRI active fire products, and to the MODIS MOD14/MYD14 active fire products using the SEVIRI-to-MODIS intercomparison methodology detailed in Section 3.1. The inter-comparison was conducted using all available FRP-PIXEL products collected over the southern African LSA SAF geographic region in August 2014 (a total of 2959), a month when fires are highly prevalent in southern Africa. For comparison we collected all the available files from the alternative SEVIRI active fire data products, a total of 2949 for WFABBA (Prins *et al.,* 1998), 2963 for FDeM product (Amraoui *et al.,* 2010), and 2914 for FIR (Joro *et al.,* 2008). Due to various data collection and processing issues, not all products were available for all SEVIRI source scenes, as is evident from the slightly different (max 1.5%) number of products in each case. Also, each product has different classes of output, and the FIR product for example classifies fire pixels as either active fires or potential active fires. In this comparison we focus on only confirmed active fire detections. Similarly, the WFABBA product 'filters' active fire pixels detected only once in a 24 hour period and classes them less likely to be fires, aiming to reduce the number of false alarms detected and minimise effects due to sunglint. In our analysis of the WFABBA active fire product we therefore include four variations of the WFABBA dataset. These are the inclusion of all fire detections, all the WFABBA ‘filtered’ detections (where pixels only detected once during 24 hrs are removed) and the WFABBA ‘filtered’ detections keeping only 1) the high probablility fires (WFABBA flags 0 to 3) and 2) high and medium probability fires (WFABBA flags 0 to 4).

For comparison to the SEVIRI-derived active fire products we used 544 Collection 5 MODIS MOD14/MYD14 active fire products, acquired over southern hemisphere Africa. To facilitate comparison with the SEVIRI products, we subset the SEVIRI products to cover the same area

as the MODIS products and selected the set of temporally coincident MODIS active fire pixels that matched with SEVIRI active fire products in time (±6 minutes). The MODIS active fire pixels were remapped to SEVIRI's imaging grid and had their FRP atmospherically corrected using the same approach as detailed in Section 3.1 to match the methodology used to generate the FRP values within the FRP-PIXEL product. SEVIRI's per-pixel point spread function (PSF) at the sub-satellite point extends more than 5 km radially from the pixel centre (Wooster *et al.*, 2015), so following the approach of Freeborn *et al.* (2014a) we evaluated the SEVIRI-derived active fire detection performances against the presence of MODIS active fire pixels within a 3×3 pixel window centred on the SEVIRI active fire pixel under investigation. Again, as with Section 3.1 the comparison was restricted to MODIS active fire detections made within a ±30° scan angle (Freeborn *et al.*, 2014a).

3.2.2 Results

The MOD14/MYD14 products contained 286,000 active fire detections during August 2014 over the southern African LSA SAF geographic region, and once remapped onto the SEVIRI imaging grid, this equated to 112,576 pixels. Within the specified ±6 minute MODIS to SEVIRI imaging time limit, the FRP-PIXEL product detects 33,414 active fire pixels and 29,037 of these are also detected by the remapped MOD14/MYD14 data. This corresponds to a SEVIRI active fire pixel detection commission error of 13%. Using the same SEVIRI level 1.5 data, the WFABBA, FDeM and FIR active fire products detect 13,008, 7664 and 7151 active fire pixels respectively, and of these, 12,284, 7260 and 6730 are coincident with a MODIS active fire detection respectively. Hence, the active fire pixel errors of commission are 5.5%, 5.2% and 5.8% respectively for these three SEVIRI-derived products, active fire errors of commission rates around half those of the FRP-PIXEL product. The WFABBA filtered dataset also stratifies active fire detections according to their detection confidence. We analysed the fire detection performance of the WFABBA filtered dataset by just including medium and high probability fires (flags 0-4) and only high probability fires (flags 0-3). These filtered WFABBA datasets detect 9736 (flags 0-4) and 8832 (flags 0-3) active fires and of which 9369 and 8496 are coincident with MODIS active fire pixels. This equates to a reduced commission rate of 4 % for both whilst the omission rate increases to 87% and 88% respectively.

A summary of the SEVIRI active fire product intercomparison results is given in Table 2. The ~13% active fire error of commission rate for the FRP-PIXEL product found here and by Freeborn *et al.* (2014a) is higher than the ~8% found by Roberts and Wooster (2008, 2014) using the FTA algorithm prototype. The disparity is in part due to the differing way in which the operational FTA algorithm applies a high-pass spatial filter to screen out certain false alarms from the potential fire pixel set (Roberts and Wooster, 2008). As discussed in the companion paper that describes the fire thermal anomaly (FTA) algorithm in detail (Wooster *et al.,* 2015), the current LSA SAF implementation of the FTA algorithm (whose performance results are reported in Table 2) has some characteristics that are open to being updated, namely whether dynamic or static thresholds are used in the spatial filter applied at the end of the potential fire pixel (PFP) stage, and whether application of the cloud-edge mask is really necessary (see Wooster *et al.,* 2015 for details). We have tested these adaptations using one month of data (July, 2015) collected over the same Southern African region used to perform the evaluation reported in Table 2, and have compared the results to those from contemporaneous MODIS overpasses. Results show that with both adaptations applied, the error of commission of the adjusted FTA algorithm compared to MODIS reduce from the current 14% to 12%, whilst the error of omission remains at 70%. These two adaptions are therefore now being implemented in the operational FTA processing chain.

The minimum FRP detection limit of an active fire detection algorithm is directly proportional to the pixel area (Roberts and Wooster, 2008; Wooster *et al.,* 2015). If the active fire detection algorithm of Giglio *et al.* (2003) used to generate the Collection 5 MOD14/MYD14 MODIS active fire products were applied to SEVIRI level 1.5 imagery, the minimum FRP detection limit at the Meteosat SSP would be 70 - 80 MW, around 10× the minimum FRP detection limit of the MOD14/MYD14 active fire products due to SEVIRI's ~ 10× larger nadir view pixel area. By contrast, the design of the FRP-PIXEL product attempts to lower the minimum FRP detection limit significantly below this by detecting active fire pixels whose radiometric signals in the MWIR, LWIR and MWIR-LWIR are raised even quite minimally above that of the ambient background (Roberts and Wooster, 2008). By exploiting a variety of spectral and spatial thresholds and contextual processing methods, the FTA algorithm is sometimes capable of detecting SEVIRI active fire pixels having an FRP down to ~ 20 MW at the Meteosat SSP. Nevertheless, statistics show that for active fire pixels below ~ 50 MW the active fire pixel count is underestimated more by SEVIRI compared to the performance above this threshold (Freeborn *et al.,* 2009). However, by

restricting our comparison of the FRP-PIXEL product to active fire pixels having FRP ≥ 50 MW the active fire pixel error of commission of the FRP-PIXEL product fell only slightly to 12%, indicating that false alarms are not necessarily dominated by these low FRP fire pixels.

Whilst our analysis has shown somewhat higher active fire errors of commission for the FRP-PIXEL product compared to the WFABBA, FIR and FDeM products, we find the latter have much higher active fire errors of omission. Figure 4 illustrates the variation seen in active fire pixel detection performance between the different SEVIRI products for one imaging slot (21st August, 2014, 13:15 UTC). In this example, the FRP-PIXEL, WFABBA, FDeM and FIR products detect 1249, 686, 346 and 312 active fire pixels respectively, illustrating a substantial degree of difference. Furthermore, the fire diurnal cycle retrieved using the four products from a single day of data shown in Figure 5 highlights the fact that these differences are maintained over the course of the day, leading to very large variations in the total count of active fires detected on a daily basis.

When compared to the matching MODIS active fire pixel detections, the WFABBA, FDeM and FIR products contain active fire pixel detections that match 16%, 8% and 5% respectively of the MODIS active fire pixels, whereas the figure for the LSA SAF FRP-PIXEL product is substantially higher at 23%. Georgiev and Stoyanova (2013) previously undertook a limited study of the FRP-PIXEL product performance in south-east Europe, and determined that it provided a marginally higher active fire detection efficiency than did the FIR product. Using a wider area of a region with many more fires covering a wide FRP range we find much larger differences, and indeed the FIR product appears to provide the worst performance of all the four SEVIRI products in terms of its ability to detect active fire pixels. Restricting the FRP-PIXEL active fire detections to those pixels ≥50MW, the FRP-PIXEL product still detects 9896, 14864, 15896 more active fire pixels that are coincident with MODIS than do the WFABBA, FDeM and FIR products respectively. This corresponds to active fire pixel count differences in excess of ~ 175%, even when limiting the detection regime to an FRP range where all the SEVIRI-derived products should in theory be able to show a reasonably strong performance.

Our analysis of the operational FTA algorithm's performance has shown an active fire pixel error of omission rate of 77% when comparing the FRP-PIXEL product to simultaneously collected MODIS active fire pixels. This omission error is similar to that previously found by

Roberts and Wooster (2014) and Freeborn *et al.* (2014a) for the FTA algorithm, and primarily results from the ~ 10× larger nadir pixel area of SEVIRI than MODIS. In comparison, the errors of omission for the WFABBA, FDeM and FIR products are significantly greater, at 84%, 92% and 95% respectively. Restricting the comparison to those FRP-PIXEL product pixels having a SEVIRI-retrieved FRP ≥ 50 MW, which SEVIRI-based algorithms should be able to detect quite readily, reduces the FRP-PIXEL product active fire pixel error of omission to ~50% in comparison to MODIS.

In terms of FRP measurements, the ratio between the total cumulative FRP measured within the same southern African geographic region covered by the near-simultaneous FRP-PIXEL and MODIS active fire products is 0.48. This represents a lower underestimate of FRP than might be expected from the FRP-PIXEL omission error rate, and the reason is that the unidentified active fire pixels are predominantly those having low FRP values (<< 50 MW). Restricting the analysis to only those active fires that are correctly identified by both products provides a cumulative FRP ratio of 0.96, showing an excellent agreement in the regional FRP assessment when only active fires successfully detected by both sensors are taken into account. This agrees with the strong-performance in terms of per-pixel FRP assessment seen in Section 3.1.

Certain previous studies evaluating the FTA algorithm or prototype FRP-PIXEL datasets (e.g. Roberts and Wooster, 2008; Xu *et al.*, 2010; Roberts and Wooster, 2014) have applied an alternative approach when comparing these to MODIS active fire datasets. Rather than the per-pixel approach to inter-comparison applied above, Freeborn *et al.* (2014a) grouped active fire pixels into contiguous clusters based on their spatial closeness to other active fire pixels in the same manner as that described in Section 3.1 for the per-fire FRP intercomparison. To strengthen the link between this work and these previous findings, active fire pixels within each of the active fire products tested were also clustered into spatially contiguous groupings, and the active fire detection errors of commission and omission calculated based on a ‘fire cluster’ basis instead of for the individual fire pixels. We used a similar strategy for this inter-comparison as used at the pixel scale, specifically searching the surrounding 3 × 3 pixels for matching active fires in the products to be compared. Using this 'clustering' approach, we found the error rates of the FRP-PIXEL product to be higher than those determined using the per-pixel approach, with errors of commission and omission of 19% and 85% respectively when compared to the matching MOD14/MYD14 products. Again, if only those fire clusters

having an FRP ≥ 50 MW are included, these reduce to 18% and 57% respectively, demonstrating in particular a high success of active fire detection in this region of the FRP regime. Using the same approach with the alternative SEVIRI active fire products, we find that the WFABBA products also show slightly higher errors of omission and commission than when examined at the fire cluster scale, now being 7% (commission) and 90% (omission) respectively in comparison to the MODIS product. The error rates for FDeM and FIR products are, however, very similar when examined on a fire cluster basis to the results on a per fire pixel basis, with a commission rate of 6% for both and an omission rate of 96% and 95% for FDeM and FIR respectively.

4. FRP GRIDDED Product Evaluation

4.1 Method

Section 2.2 detailed how the LSA SAF SEVIRI FRP-GRID product uses a series of regionally-specific bias adjustment factors (α) to upwardly adjust regional FRP estimates for e.g. the impact of undetected low FRP fire pixels. The aim is to produce an hourly, regional FRP estimate that has minimal bias compared to if MODIS had been able to view the same area at the same time. Full details of the FRP-GRID processing chain are included in Wooster *et al.* (2015). We evaluated the performance of the applied bias adjustments using a validation dataset composed of coincident SEVIRI and MODIS observations collected between May 2008 and May 2009 in each of the four LSA SAF geographic regions. Boundaries of the relevant MODIS level 2 swath products were used to identify all MODIS granules that intersected each region during the year-long study period, and fire pixels subset from the full MODIS 'MOD14' and 'MYD14' products using six, non-overlapping 5.0° grid cells arranged in the centre of each MODIS granule (Figure 6). Active fire pixels detected by MODIS outside of this region of interest were discarded and not used during the analysis. The sampling design ensured complete coverage of the 5.0° grid cells regardless of the MODIS ground track, and also mitigated the effects of image distortion at the edge of the MODIS swath. All MODIS granules collected during the year-long study period were matched to the most concurrent SEVIRI image, always within ±6 minutes of each other. The same 5.0° grid cells inscribed within the MODIS granule were then used to clip SEVIRI fire pixels from both (i) the most coincident SEVIRI timeslot, and (ii) the three SEVIRI timeslots immediately preceding the MODIS overpass. Again, active fire pixels detected by SEVIRI

outside of this region of interest were not included in the analysis. Entire grid cells were also discarded if three consecutive SEVIRI imaging timeslots could not be retrieved prior to the SEVIRI timeslot concurrent with the MODIS overpass (i.e., if four imaging timeslots were not available). This sampling design not only permitted a genuine comparison of coincident SEVIRI and MODIS observations of FRP, but also mimicked the hourly temporal resolution of the gridded FRP product.

After the SEVIRI and MODIS fire pixels were spatially and temporally accumulated, half of the concurrent and collocated 5.0° grid cells in each region were used to generate the validation dataset. Relationships between the atmospherically corrected FRP observed by SEVIRI and MODIS were directly compared among the 5.0° grid cells contained within this dataset. Rather than using the instantaneous FRP observed by SEVIRI at the timeslot most concurrent with the MODIS overpass however, the mean FRP generated from the SEVIRI data available over the preceding hour was used instead to correspond more appropriately with the hourly resolution of the FRP-GRID product.

4.2 Results

A complete summary of the FRP-GRID product validation results derived from the methodology detailed in Section 3.1 is provided in Table 3. Application of the weighted least squares (WLS) coefficients in northern and southern Africa to the validation dataset yielded unbiased estimates of the instantaneous FRP that would have been measured by MODIS at 5.0° spatial resolution (e.g., Figure 7a, Table 3). As expected, however, the region-specific coefficients for South America (Same) and Europe (Euro) geographic regions did not perform as well. Although the adjustment procedure provides an unbiased estimate of the FRP that MODIS would have measured in South America, the coefficient of determination (r^2) indicates that confidence in the predictive capability of the model is limited at this spatial and temporal resolution. As a caveat, however, the validation results in South America and Europe are influenced by observations when SEVIRI did not detect a single active fire pixel within a 5.0° grid cell during the hour. After removing 5.0° grid cells that only contained an active fire pixel detected by a single sensor (i.e., thereby forcing a comparison between observations in which both SEVIRI and MODIS viewed a fire) the r^2 improved to 0.43 in the South America region. Furthermore, by removing a lone outlier improved the correlation

coefficient slightly further to 0.55. Likewise for Europe, only including observations in which SEVIRI and MODIS simultaneously detected an active fire pixel yielded an r^2 of 0.31.

Of course, the linear bias adjustments applied in the FRP-GRID product only capture the underlying macroscopic features of the sensor-to-sensor relationships, and do not account for any temporal variability in the SEVIRI-to-MODIS ratios of FRP induced by diurnal or seasonal fluctuations in fire activity (e.g. as seen in Freeborn *et al.*, 2009). By deriving different regression coefficients for each of the four LSA SAF regions, however, the FRP-GRID algorithm does account for broad spatial differences in the sensor-to-sensor relationships that potentially arise from (i) differences in fire regimes, and (ii) differences in SEVIRI view zenith angles.

To assess the predictive capability of the bias adjustment factors at broader spatial and temporal scales than simply the hourly/5° spatio-temporal resolution of the FRP-GRID product, the SEVIRI and MODIS validation data were accumulated over weekly intervals and comparisons were performed at scale of the LSA SAF geographic regions. Figure 7b illustrates that in southern Africa, the bias adjustment factors used to generate the FRP-GRID product consistently underestimate the weekly sum of FRP measured by MODIS across this region, and that these results are typical of all four regions (Table 3). Again, this systematic underestimation is partly attributed to the challenge of performing a bias adjustment when SEVIRI does not detect a fire pixel (i.e. the linear bias adjustment coefficient is then applied to an FRP of zero). Nevertheless, the weekly/regional biases shown in Table 3 could in turn be used to adjust the SEVIRI FRP-GRID product measurements to deliver unbiased estimates of the FRP that would have been measured by MODIS at the regional/weekly scale.

5. EXAMPLE APPLICATION OF THE LSA SAF METEOSAT SEVIRI FRP PRODUCTS IN THE COPERNICUS ATMOSPHERE MONITORING SERVICE (CAMS)

5.1 Introduction to FRP-PIXEL Product use in Atmospheric Transport Models

From the FRP-PIXEL product evaluation and inter-comparison conducted in Section 3 it is apparent that the FRP-PIXEL product detects a larger proportion of the ‘true’ landscape-scale fire activity than do alternative SEVIRI-derived active fire products, albeit with a higher

commission rate. That evaluation also highlighted the failure of the FRP-PIXEL product to detect many of the actively burning fires that MODIS would detect, particularly the lower FRP fires, resulting in an overall omission rate of 77% over the four geographic regions (Table 1). The degree of difference between geostationary and polar-orbiting active fire products does, however, vary with factors such as geographic location, season and time of day (which all influence the type of fire regime and its subcomponents being sampled), sensor viewing geometry, land cover heterogeneity, fire detection algorithm and the quality of ancillary data such as cloud masks (Freeborn *et al.*, 2014a; Schroeder *et al.*, 2008; Roberts and Wooster, 2014; Xu *et al.*, 2010). Indeed, under some conditions, geostationary active fire datasets compare rather favourably against those derived from polar-orbiting sensors. Georgiev and Stoyanova (2013) analysed a series of short–lived wildfires in south-eastern Europe with the FRP-PIXEL product, and found the higher temporal resolution of SEVIRI resulted in a 50% lower active fire omission rate than did the use of MODIS. Wooster *et al.* (2015) also demonstrate that, taking the Central African Republic as an example, most fires detected by the MODIS are detected by the SEVIRI FTA algorithm, just not necessarily at the same time as the fire is detected by MODIS. Indeed, the high temporal frequencies offered by geostationary observations can enable the diurnal fire cycle and related short-term changes in fire activity to be far better characterised than with polar-orbiting data, and this ability is starting to be exploited to parameterise wildfire emissions in atmospheric transport models.

One such example is provided by Baldassarre *et al.* (2015), who used the FRP-PIXEL products (Wooster *et al.*, 2015) and the WFABBA SEVIRI products (Zhang *et al.*, 2012), along with MODIS-derived information from the Global Fire Assimilation System (GFAS) inventory of Kaiser *et al.* (2012), to derived biomass burning emissions inputs for simulations of emissions from a large fire in Turkey (Antalya, 2008). The FRP-PIXEL product provided by far the most accurate description of the emissions, both with regard to their spatio-temporal variation and their absolute magnitude. Unlike the MODIS-derived GFAS inventory, the SEVIRI FRP-PIXEL product was able to capture the fires complete life cycle, including the time of peak emissions intensity. And compared to the WFABBA product, the FRP-PIXEL product produced information more consistent with that from MODIS when both SEVIRI and MODIS viewed the Antalya region simultaneously. The simulated smoke plume produced by ingesting the FRP-PIXEL data into the Community Multi-scale Air

Quality (CMAQ) atmospheric chemistry model compared far better with observations of MODIS-derived aerosol optical depth (AOD), and with carbon monoxide and ammonia column totals provided by the Infrared Atmospheric Sounding Interferometer (IASI), in particular in relation to the diurnal variability of the fire emissions and the spatial distribution and peak concentrations of the smoke. Please refer to Baldassarre *et al.* (2015) in this Monitoring Atmospheric Composition and Climate (MACC) special issue for further information on the simulation and inter-comparison. Here we provide a second European demonstration of the value of geostationary FRP data in the parameterising of wildfire emissions for use in atmospheric transport models, building on a previous more limited study conducted by Kaiser *et al.* (2009b).

5.2 Methodology for modelling emissions and transport of smoke from the 2007 Greek 'mega fire' event

We use the FRP-PIXEL product as the basis for calculating smoke emissions to the atmosphere from a catastrophic 'mega fire' event that occurred around the Mediterranean, in particular focused on the Greek island of Peloponnese, in August and September 2007. We use these emissions within components of the CAMS modelling systems to simulate the transport and fate of the emitted smoke, ultimately estimating the level of human exposure to high levels of particulate matter (PM2.5). The Peloponnese wildfires occurred after a period of prolonged drought (Gitas *et al.,* 2008), and during a heatwave (Theoharatos *et al.,* 2010). The MODIS burned area product (Roy *et al.,* 2005) indicates they burned across an area of around 1847 km^2 (Figure 8), a figure in good agreement with burned area reports provided by the local Hellenic fire brigade (1899 km^2). The Peloponnese fires predominantly occurred in forested land, both coniferous and broadleaved forest, though some areas of shrublands, grasslands and olive groves were also affected (Veraverbeke *et al.,* 2010; Koutsias *et al.,* 2012). Such was their severity that 0.32 Tg (40 %) of the estimated mean annual carbon monoxide (CO) emissions for Greece overall were estimated to have been released by these fires alone (Turquety *et al.,* 2009). The fires contributed greatly to reductions in local air quality, with PM10 values in Athens reaching almost 100 µg m^{-3}, double that of the European Union Ambient Air Quality Standard for daily PM10 (50 µg m^{-3}). Outside Athens at a background non-urban site, on 24-25th August the PM10 concentration rose to 49 µg m^{-3}, significantly up from the 19 µg m^{-3} measured the day before (Liu *et al.,* 2009). Marlier *et al.* (2014) and Reid *et al.* (2009) have already highlighted the potential improvements that high

765 temporal resolution source information can have on the modelling of biomass burning
766 emissions transport, and the exceptional and strongly varying intensity of the Peloponnese
767 fires provides an excellent opportunity to demonstrate this further using SEVIRI-derived FRP
768 observations.
769
770 **5.2.1** ***Derivation of smoke emissions fields from FRP-PIXEL data***
771
772 FRP-PIXEL data of the European LSA SAF geographic region collected between the 1st
773 August and 13th September 2007 was examined for signals of the fires that occurred around
774 the Mediterranean during July - Aug 2007. Clear FRP signals were apparent from these fires,
775 particularly those on Peloponnese, but it was also evident that the adjusted version of Cloud
776 Mask (CMa) of Derrien and Le Gleau (2005) delivered by the Nowcasting and Very Short
777 Range Forecasting SAF (NWC SAF; www.nwcsaf.org) and used within the FRP-PIXEL
778 product processing chain (Wooster *et al.,* 2015) was identifying some of the extremely thick
779 smoke emitted by these fires as cloud. This is appropriate for studies requiring clear sky
780 observations, but the sensitivity of the algorithm for detecting cloud or smoke contaminated
781 pixels can occasionally result in the omission of fire activity. Since cloud masking is one of
782 the first things conducted within the FRP-PIXEL product processing chain (Wooster *et al.,*
783 2015), misidentification of very thick smoke as cloud prevents fires being identified in these
784 pixels using the FTA algorithm, even though we know that active fires can be quite reliably
785 detected through even quite thick smoke (Petitcolin and Vermote, 2002). This is because
786 smoke particles have a diameter typically much smaller than the wavelength of the MWIR
787 band and so do not act as strong scatterers of the fire-emitted radiation, unlike meteorological
788 cloud (Kaufman and Remer, 1994). Analysis of the raw SEVIRI level 1.5 data, along with the
789 EUMETSAT Meteorological Product Extraction Facility (MPEF) cloud mask (Tjemkes and
790 Schmetz, 1997), confirmed the identification of some areas of thick smoke as cloud by the
791 CMa cloud mask, and also confirmed that the true median percentage cloud cover over
792 Peloponnese was low over the period of the mega fire event (13%). To prevent the masking
793 out of smoke covered fires, which also then impacts surrounding pixels due to the single pixel
794 wide mask that is applied around cloud and water pixels (Wooster *et al.*, this issue), for this
795 particular application we decided to turn off the use of the adjusted CMa cloud mask, and
796 simply relied on the basic cloud masking tests used within the FTA algorithm itself (Wooster
797 *et al.,* 2015). Currently investigations are ongoing to make the cloud masking within the

FRP-PIXEL product less sensitive to thin cloud and other atmospheric phenomena through which fires can still be identified, including very thick smoke (Wooster *et al.*, 2015).

We then gridded the FRP data from within the FRP-PIXEL product to 0.1° grid cells and calculated the mean FRP for each cell at an hourly temporal resolution. As with the operational version of the Global Fire Assimilation System (GFAS; Kaiser *et al.*, 2012), the FRP density ($\tilde{\varrho}_j$, Wm^{-2}) for each cell was then calculated by normalising the measured FRP by the grid cell area (a_j, m^2):

$$\tilde{\varrho}_j(d,h) = \frac{1}{a_j}\frac{1}{4}\sum_{k=0,15,30,45}\sum_{i_k \in j} F_{ik}(d,h) \qquad (1)$$

where d,h and k are the date, hour and minute of the SEVIRI observations respectively, $\sum F_{ik}$ is the summation of all FRP measurements within grid cell j.

The rate of dry matter (DM) fuel consumption (φ [kg s^{-1} m^{-2}]) was derived from the FRP density measures of each grid cell ($\tilde{\varrho}$, Wm^{-2}) following the method described in Wooster *et al.* (2005):

$$\varphi\,(d,h) = c \times \tilde{\varrho}\,(d,h) \qquad (2)$$

where d is the day, h is the hour and c is the conversion factor that relates fuel consumption to FRP and which is 0.368± 0.015 (kg MJ^{-1}; Wooster *et al.*, 2005). The approach was further developed with land cover dependent adjustments by Kaiser *et al.* (2012). However, we maintain the original fuel consumption estimation and adjust the emission fluxes at the level of the emission factors, see section 5.2.2.

5.2.2 *FRP-derived aerosol emissions and atmospheric modelling*

Ichoku and Kaufmann (2005) first developed an approach to estimate aerosol emissions using FRP and aerosol optical depth (AOD) measurements using '*coefficients of emission*' that related FRP to total particulate matter (TPM) as a function of land cover type. The approach implemented herein calculates emissions using the DM fuel consumption rate φ (kg s^{-1} m^{-2}):

$$\Phi_s(d,h) = \eta_s \times \varphi(d,h) \qquad (3)$$

where Φ_s is the emission flux density (kg s^{-1} m^{-2}) of species s, d is the day, h is the hour and η is the emissions factor (kg kg^{-1}) given by :

$$\eta_s = \alpha(s) \times \kappa_l(s) \qquad (4)$$

where κ_l is the land cover (l) specific emissions factor for species s and α is a constant which is used to adjust bottom-up aerosol emissions estimates to those observed in top-down inventories. A regionally varying bias occurs between bottom-up derived aerosol emissions and MODIS AOD measurements, requiring the former to be adjusted when being used in air quality or climate model simulations (Peterenko *et al.*, 2012). Yang *et al.* (2011) also found smoke emissions ($PM_{2.5}$) derived using the bottom-up approach was underestimated by a factor of three when compared to MODIS AOD retrievals. Kaiser *et al.* (2012) recommend a global aerosol enhancement by a factor of 3.4 as first-order correction. These values are also broadly consistent with differences of up to a factor of three found by Ichoku and Kaufmann (2005) using satellite observations of FRP and AOD compared to measurements of $c \times \kappa_l(s)$ derived from laboratory measurements. Here, we estimate emissions of organic matter and black carbon in exact agreement with Ichoku and Kaufmann (2005) by enhancing their emission factors for Andreae and Merlet (2001) with a factor of 3.1. According to the GFEDv3 land cover dataset, also used for our calculations in GFAS (Kaiser *et al.*, 2012), the fire affected region of Greece is classed as extratropical forest and the emitted species and relevant emissions factors are given in Table 4.

The atmospheric aerosol model (Morcrette *et al.*, 2008) used within the ECMWF Integrated Forecasting System (IFS) represents smoke aerosols as black carbon (BC) and organic matter (OM), of both hydrophilic and hydrophobic types. Emissions of the latter are approximated by scaling organic carbon (OC) emissions estimates by a factor of 1.5. Other aerosols included in the modelling are sea salt, dust and sulphate aerosols, and advection, convection, diffusion, dry and wet deposition and chemical conversion of these aerosols are simulated, with meteorology nudged to the operational ECMWF analysis every 12 hours. The aerosol abundance however, is based solely on source and sink processes and the atmospheric

transport. In this study the IFS model was run with a horizontal resolution of 25 km (T799) and with 91 vertical levels up to 0.01 hPa.

Smoke emissions from the Peloponnese fires were calculated using Equations 3 and 4, along with the emissions factors given in Table 4. The smoke emissions must be injected into the atmosphere at a particular height, or distribution of heights, and such injection height assumptions can have implications for the resulting spatio-temporal distribution of the emitted species. Leung *et al.* (2007) and Guan *et al*. (2008) demonstrated that use of more detailed plume injection height assumptions resulted in a reduction in near surface CO concentrations, since more plumes were assumed to be lofted above the boundary layer. Paugam *et al.* (2015a) provided a recent review of approaches to estimate smoke plume injection height, including the methods of Sofiev *et al.* (2012) and Paugam *et al.* (2015b) that use FRP measurements to characterise wildfire thermal properties related to plume rise. This research remains at a relatively early stage, but it appears that FRP measures may indeed have a role to play in characterising smoke plume injection height as well as the rate of emission of chemical and aerosol species. Here we retained the commonly used assumption that the calculated smoke emissions are injected into the lowest atmospheric level, since this is generally what has been assumed in the series of MACC projects thus far (Kaiser *et al.,* 2012). The CAMS is anticipated to use injections heights from Paugam *et al.* (2015b) in the future.

5.3 Results

5.3.1 Fuel consumption during the Peloponnese Wildfires

Figure 9a illustrates the temporal dynamics of total fire FRP (MW) and the equivalent rate of fuel consumption (tonnes s^{-1}), calculated from the MODIS and SEVIRI FRP measurements at their native temporal resolutions. The period of greatest fire activity occurs between the 23rd and 27th August, where the initial active fire detections made by SEVIRI and MODIS occur at 07:57 and 09:00 (UTC) respectively (23rd August). At their most intense, the Peloponnese fires consumed over 15 tonnes s^{-1} of biomass, and such was their intensity that large quantities of fuel (> 3 tonnes s^{-1}) were consumed even during the night, a period when more landscape typically fires die down quite considerably due to less fire-conducive ambient conditions (Roberts and Wooster, 2007; Roberts *et al.,* 2009). The temporally intermittent

MODIS Terra and Aqua FRP measurements broadly capture the pattern seen in the much more frequent SEVIRI data, and are typically much higher in magnitude. On the 25th August, MODIS Aqua (12:05 UTC) detects a total FRP exceeding 180 GW, with the SEVIRI FRP (12:12 UTC) very much lower (38 GW). The large difference mainly derives from the fact that whilst 10% (31) of the MODIS active fire pixels have an FRP >1600 MW and 5% >3000 MW, 23% of the 100 active fire pixels detected by the FRP-PIXEL product are in fact saturated in the SEVIRI MWIR channel. Between the 24th and 26th August, when the wildfires were most intense, MODIS made 13 overpasses and the unadjusted SEVIRI observations measured 39% of the total FRP measured by MODIS. This demonstrates the massive scale and intensity of these fires, particularly given that SEVIRIs pixel area at this location is around 14 km^2.

Temporal integration of the SEVIRI FRP measurements between the 23rd August and 3rd September indicates an energy release of 4.73 PJ which, following Equation 2, equates to 1.74 Tg of combusted fuel, predominantly consumed on 23 - 27 August (Figure 9b). Various burned area estimates exist for the Peloponnese fires, including 1773 km^2 (Gitas *et al.,* 2008), 1628 km^2 (European Forest Fires Information System, EFFIS; European Commission, 2010) and 1847 km^2 (Roy *et al.,* 2005; Figure 8). Dividing the SEVIRI-FRP derived fuel consumption with these burned areas provides mean dry matter (DM) fuel consumptions of 0.98 kg m^{-2}, 1.07 kg m^{-2} and 0.94 kg m^{-2} respectively. Aleppo pine forests occupy around 370,000 ha in Greece and are abundant on Peloponnese (Verroios and Georgiadis, 2011). Mitsopoulos and Dimitrakopoulos (2013) assessed 40 stands in this fuel type and found canopy fuel loads to range between 0.63 and 1.82 kg m^{-2}, estimating a mean of 1.08 kg m^{-2}. Using the maximum fuel load (1.82 kg m^{-2}), the three burned area estimates (1773 km^2, 1628km^2 and 1847km^2), and assuming a combustion completeness value for forest of 0.6 (van der Werf *et al.,* 2006) we calculated a fuel consumption for these fires of 1.94 Tg, 1.77 Tg and 2.01 Tg respectively using the standard burned area based approach (Seiler and Crutzen, 1980), which is simular to our SEVIRI-derived estimate of 1.74 Tg. Turquety *et al.* (2009) estimates that 0.32 Tg of CO was emitted during the Peloponnese fires, which using the emissions factors given in Table 4 results in a larger top-down derived fuel consumption 3.0 Tg (with a stated uncertainty of ~30%). Due to the aforementioned SEVIRI MWIR channel saturation, the SEVIRI FRP-derived fuel consumption estimate is considered a minimum estimate.

927 **5.3.2** ***Smoke Plume Evolution***

928

929 The Peloponnese wildfires produced huge volumes of smoke that affected regional air quality
930 in the Eastern Mediterranean (Poupkou *et al. 2014)*. Figure 10a shows a true colour
931 composite image derived from MODIS Terra imagery acquired on the 26th August 2007
932 (09:35 UTC). The mirrored 'S' shaped plume present over the Mediterranean extends across
933 to Tunisia at this time. Figure 10b shows a snapshot of the modelled smoke emissions derived
934 from our use of the FRP-PIXEL product dataset to derive the wildfire emissions, and the use
935 of these within the IFS model (Section 5.2). The modelled smoke emission transport captures
936 the spatial structure of the advected smoke plumes very well, consisting of a series of 'pulses'
937 of increased AOD that result from the particularly intense emissions during the peak of each
938 diurnal fire cycle. The large region of particularly high AOD on the coast of Libya (L on
939 Figure 10b, and shown in Figure 11a and 11b) results from the intense fire emissions on the
940 25th August, where more than 18 tonnes s^{-1} of biomass were apparently being consumed at the
941 peak intensity. To the west of the main smoke plume, a thinner plume with a lower AOD is
942 evident emanating from fires in Albania. To the east, a smaller plume resulting from wildfires
943 in Turkey is also captured.

944

945 It is evident from Figure 10 that the modelled smoke plumes are offset slightly compared to
946 the actual plumes observed by MODIS, and this is most evident over the Libyan coast. The
947 difference is believed to result from injecting the smoke plume into the lowest atmospheric
948 level, which is an oversimplification as stated earlier since MISR-derived smoke plume
949 heights acquired on 26th August indicated that the plume closest to the wildfires had a height
950 of 2.5 km (Lui *et al.*, 2009) and CALIPSO lidar observations have detected the plumes at
951 altitudes of 2-3 km on 25th and 26th August (Turquety *et al.* 2009). In contrast, the simulated
952 plumes are located predominantly below 1 km (not shown). Global analysis of MISR data
953 indicates that a large proportion wildfire smoke plume heights remain beneath the boundary
954 layer, although particularly intense fires can inject smoke into the free troposphere (Val
955 Martin *et al.*, 2010; Dirksen *et al.*, 2009; Fromm *et al.*, 2000). Our modelled plume is
956 typically also broader than that observed by MODIS, and covers a larger spatial extent. This
957 may result from the relatively coarse spatial resolution used in the model, and comparisons
958 between our simulation and MODIS AOD estimates made on the 26th August (DOY 238,
959 Figure 11a and b) indicate that whilst the broad magnitude of the modelled smoke emission
960 'pulses' are in good agreement with observations, the simulated plumes AOD appears

961 overestimated compared to MODIS. This suggests some inaccuracies remain in the aerosol
962 source modelling, and for example Garcia-Menendez *et al.* (2014) found modelled $PM_{2.5}$
963 concentrations are more sensitive to the injection height parameterisation rather than to the
964 emissions vertical distribution, due to the diurnal evolution of the planetary boundary layer
965 and local meteorological conditions.
966
967 **5.4. Impact of Emissions Fields Temporal Resolution**
968 A number of studies (e.g. Chen *et al.*, 2009; Marlier *et al.*, 2014; Reid *et al.*, 2009; Garcia-
969 Menendez *et al.*, 2014) have found that resolving the diurnal variability of fire emissions has
970 important implications when modelling the emissions atmospheric transport. We used our
971 study of the Peloponnese fires to address this issue by reducing the temporal resolution of the
972 SEVIRI FRP-derived emissions density fields, from the original 1-hour to 1-day and then 1-
973 week, the latter two being more representative of the global emissions inventories developed
974 using only observations from polar orbiting instruments (van der Werf *et al.,* 2010; Kaiser *et*
975 *al.,* 2012; Sofiev *et al.,* 2009). The resulting sensitivity to temporal resolution is illustrated in
976 Figure 12a and b, which show modelled AOD (at 550nm) on the 26th August (09:35 UTC)
977 using the emissions prescribed at a daily and weekly temporal resolution. In both cases, the
978 shape of the modelled Peloponnese smoke plume remains broadly consistent with the hourly
979 simulation of Figure 10a, although smoke emissions from neighbouring countries are much
980 less pronounced. The Albanian plume is progressively shorter in Figure 12a and 12b, whilst
981 some plumes (e.g. those from Turkey to Crete) are missing altogether. Source emissions at
982 weekly temporal resolution (Figure 12b) remove the daily variability, resulting in lower
983 aerosol amounts at both the source region and over the entire plume. It is also evident that
984 emissions are being generated at incorrect times when using these reduced temporal
985 resolution source data. For example, the daily and weekly simulations have plumes
986 emanating from southern Italy too early, since fires are in fact in reality just developing in the
987 source region (Figure 12b). Baldassarre *et al.* (2015) provide further evidence of the
988 importance of the high temporal resolution provided by the SEVIRI FRP-PIXEL dataset
989 when modelling smoke transport from individual large fire events.
990
991 **5.5 Comparison of *in-situ* and modelled aerosol optical depth**
992
993 Section 5.4 has indicated that model simulations using hourly smoke emissions fields
994 improve the representation of both the spatial and temporal evolution of the smoke plumes

from the main Mediterranean mega-fires of August 2007. However, qualitative comparison to MODIS AOD estimates (Figure 11 a,b) indicated that the plumes modelled AOD was somewhat higher than satellite derived AOD estimates. Over the same time period as the Peloponnese fires, a series of fires occurred on the Algerian coast (Figure 13a) whose plumes were detected by the AERONET (Holben *et al.*, 2001) site at Lecce (Italy; 40.35°N, 18.16°E). Figure 13b and c show the modelled smoke and dust AOD respectively on the 31st August (00:00 UTC) where the former illustrates the smoke plume extension over the AERONET site (yellow star symbol). Figure 13d is a temporal profile of AOD recorded (at 500 nm) over Lecce from AERONET observations of total (red circles) and fine mode (orange circles) AOD, daily averaged MODIS AOD (550 nm) observations (black triangles) and model simulations of total AOD (blue line). Modelled AOD contributions of smoke (purple line) and dust (green line) to the total AOD are also shown. The MODIS AOD estimates are derived through averaging all observations within the model grid cell. The smoke AOD displays greater short term variability than does the dust AOD, since the wildfires represent significantly more localised sources than do the regions of dust uplift. The smoke AOD displays an increase in magnitude from 0.6 to 1.3 between the 31st August and 1st September, which occurs 23 hours prior to the peak FRP (63 GW) of the Algerian fires. However, between the 27th and 31st August, MODIS detected 330 active fires in southern Italy (Figure 14) which were greatest in number on the 27th (114) and 31st (110) August and which are likely to have contributed to the Algerian smoke plume but which may not all be included in our modelling since the majority (63%) had an FRP <30 MW and so may not be detected by SEVIRI.

Compared to the daily averaged MODIS AOD, our modelled total AOD is typically overestimated by ~20% during the overpass of the smoke plume (31st August), but the model does capture the temporal trend of the observed AOD rather well. The AERONET AOD data provides a more complete temporal profile than do MODIS' AOD observations, and our modelled total AOD typically captures these dynamics. However, the onset of increased AOD due to the Algerian fires (30th August) is captured 8 hours earlier by AERONET than by our modelled AOD, whilst the descending limb is temporally coincident between datasets. The former may result from assumptions made regarding the smoke plume injection heights, or to shortcomings in the simulations due to increased cloud cover over Algeria on the 29th August. It is also possible that, given the rapid rise in AOD in a three hour period, this is a localised effect due small, undetected fires in the vicinity of the AERONET station and

which are not represented in our simulation. Between the 28th and 29th August, MODIS detected 96 active fires (Figure13, red symbols) to the south-west of Lecce and in close proximity to the smoke plume emitted by the Algerian fires, and these most likely to contribute to the elevated AOD at this time (Figure 11a and b). In general, the AOD resulting from the use of the SEVIRI FRP-PIXEL product data and the IFS model is overestimated compared to AERONET observations by 10 - 40% during the biomass burning plume overpass, and with a discrepancy of 8 hours at the onset of the plume overpass. Clearly we will in future aim to further refine the fire emissions parameterisation, which appears currently to be positively biased relative to the observations. Nevertheless, this case study has demonstrated the clear value of the high temporal frequency SEVIRI-derived FRP observations for large, rapidly varying wildfires such as this.

5.6 Air quality assessment

The 2007 Mediterranean 'mega fire' event significantly impacted regional air quality, and fires worldwide are known to have severe health implications for those badly affected by their emissions. Jacobson (2014) estimated that average annual premature mortalities due to biomass burning emissions of $PM_{2.5}$ and ozone are of the order of 20,000 (10,000-30,000) and 230,000 (63,000-405,000) respectively, equating to between 5 and 10% of global mortality due to indoor and outdoor air pollution. One of the primary uses of the CAMS is to forecast regional air quality across Europe, providing rapid and reliable information directly relevant to human health issues, and this includes the consequences of wildfire emissions (Hollingsworth *et al.*, 2008). It is therefore pertinent to assess the significance of our Peloponnese smoke emissions transport simulations in relation to air quality and human health, potentially since Mitsakis *et al.* (2014) already estimated that over 2000 people were admitted to hospitals and medical centres as a direct result of the Peloponnese fire event, and of these 1100 were due to cardio-vascular and respiratory problems. The World Health Organisation (WHO) air quality guidelines (WHO, 2006) in particular set a limit of 25 $\mu g\ m^{-3}$ for the concentration of fine mode particulate matter ($PM_{2.5}$) averaged over a 24 hour period. We estimated concentrations of $PM_{2.5}$ using our simulated OM and BC concentrations in the lowest modelled atmospheric layer, and calculated the 24-hour running average for comparison to this WHO threshold.

Figure 15 shows the distribution of 24-hour mean $PM_{2.5}$ concentrations modelled between 23rd August and 3rd September (when the Peloponnese wildfires were at their most intense;

Figure 9a). It is clear that the impacts of the Peloponnese wildfires extend well beyond Greece's national borders, and indeed resulted in large parts of the Mediterranean region exceeding the WHO 25 μg m^{-3} $PM_{2.5}$ concentration threshold by significant margins. In fact, analysis of the spatial distribution of these data with respect to population density (CIESIN and CIAT, 2005) indicated that, for the region shown in Figure 15, up to 40 million people might have been subject to $PM_{2.5}$ concentrations exceeding the WHO guidelines. However, it should be stressed that this is an upper limit for the exposure, because our study significantly over-estimates near-surface smoke concentration due to the assumed boundary-layer injection of the emissions. In particular, surface $PM_{2.5}$ concentrations in regions reasonably close to the source that are well above 100 μg m^{-3} are very likely to be spurious, and Liu *et al.* (2009) report elevated non-urban values closer to 49 μg m^{-3}, albeit still at some distance from source. Nonetheless, the spatial range of the affected area, and the considerable human health impacts that these type of large wildfire events can have, highlights the necessity of modelling their smoke emissions and forecasting their atmospheric transport in the manner demonstrated here. Through such work, the CAMS and its downstream services aim at improving emergency preparedness through air quality forecasts. Geostationary FRP data are likely to be an important component of this system, particularly so as their high temporal resolution FRP data provides a unique view of the type of individual large "mega fire" event studied here, that can impact regional air quality so dramatically over short timescales.

6.0 SUMMARY AND CONCLUSIONS

This work has provided a detailed performance evaluation of the Meteosat SEVIRI FRP products available from the LSA SAF, both the full resolution FRP-PIXEL product and the reduced resolution FRP-GRID product, both available in near real time and in archived form (http://landsaf.meteo.pt/). It has also provided a detailed example of use of the former product in characterising the smoke emissions from a large European wildfire event whose smoke significantly affected the Mediterranean region as a whole, and for which we have demonstrated an ability to simulate the atmospheric transport and human health impacts at high temporal resolution.

When evaluated against the MODIS MOD14 and MYD14 active fire products, the active fire pixel detection error of commission of the FRP-PIXEL product is found to be 9% in the North African LSA SAF geographic region, and increases to higher values particularly in Europe and South America. The basis of this variation is the combination of SEVIRI's

increasing pixel area with view zenith angle away from the sub-satellite point, and the relative proportion of lower intensity and/or smaller fires in the various LSA SAF geographic regions (i.e. their fire regimes). Area-based comparisons indicate that the FRP-PIXEL product underestimates compared to simultaneously collected MODIS FRP of a region by between 35 and 89%, with the variation being again dependent upon the above factors. Underestimation is typically maximised at regions extending towards the edge of the viewing disk, furthest away from the SEVIRI sub-satellite point. However, comparison of the FRP of individual fires successfully detected almost simultaneously by both SEVIRI and MODIS indicates a strong agreement between the two FRP measurements, with the FRP-PIXEL product meeting its Target Accuracy requirements. We find that 76% of the examined simultaneously detected fire clusters had an FRP from SEVIRI within 30% of that measured by MODIS, which given the recent quantification of MODIS' FRP uncertainty (Freeborn *et al.*, 2014c) indicates good performance from the FRP-PIXEL product. Overall, minimal bias is seen between the per-fire FRP observations made by the two sensors.

When compared against that of other active fire products derived from the same Meteosat SEVIRI observations, the performance of the operational geostationary fire thermal anomaly (FTA) algorithm used within the FRP-PIXEL product (Wooster *et al.*, 2015) compares favourably. During our comparison to MODIS, the SEVIRI WFABBA, FDeM and FIR products from Prins *et al.* (1998), Amraoui *et al.* (2010) and Joro *et al.* (2008) respectively have higher active fire errors of omission, varying between 84 and 95%, as compared to the 77% of the FRP-PIXEL product. However, these alternative SEVIRI-derived active fire products do have lower errors of commission than the FRP-PIXEL product when compared to MODIS, ranging between 5 and 6% (the FRP-PIXEL product has a 13% commission error). The FTA errors of commission are currently being reduced by re-inclusion of the dynamic spatial thresholding parameters described in Section 3.2.2 that were removed from the operational FTA algorithm for computational speed, but included in the original Roberts and Wooster (2008) prototype.

The Level-3 FRP-GRID product accumulates a series of FRP-PIXEL products and provides regional estimates of mean FRP at an hourly temporal resolution and a 5.0° spatial resolution. These estimates come already adjusted for cloud cover, and for the impact of the low spatial resolution detection bias that results in SEVIRI failing to detect the lower FRP active fire pixels. Our evaluation indicates good performance of these bias corrections at the hourly,

5.0° product resolution, but evaluation of accumulated data against summed weekly MODIS FRP over the four LSA SAF geographic regions indicates that the FRP-GRID product underestimates total FRP at this scale. This largely results from the difficulty in accounting for situations where MODIS detects fire activity in a grid cell whilst SEVIRI does not, and so the bias corrections remain inactive. We provide herein some additional adjustment factors for those wishing to use the SEVIRI FRP-GRID datasets at this type of scale.

Despite their coarse spatial resolution limitations, the FRP products available from geostationary satellites offer an unprecedented high temporal resolution for studying wildfire emissions. This is a key advantage when using such data to parameterise wildfire smoke emissions within atmospheric transport models (Reid *et al.*, 2009). Here we use a version of the FRP-PIXEL product to characterise the smoke emissions from the August 2007 Peloponnese wildfires. The resulting emissions fields are used within ECMWF's Integrated Forecast System (IFS) to model the smoke emissions transport, and in particular the black carbon and organic carbon aerosols and the resulting aerosol optical depth and $PM_{2.5}$ surface concentrations. Our results support the findings of other recent studies (e.g. Garcia-Menendez *et al.*, 2014; Marlier *et al.*, 2014) in that higher temporal resolution smoke emissions estimates provide increased fidelity in the resulting smoke plume aerial distribution and optical thickness metrics than do simulations conducted using daily or weekly temporal resolution data. Visual assessment of the modelled plumes spatial distribution against simultaneous MODIS optical imagery shows good agreement, but the modelled plume is slightly offset from the observations which is believed to result from injecting the plume into the lowest atmospheric layer (whereas in reality it would have been lofted to higher altitudes). Quantitative comparisons between our modelled AOD and the coincident MODIS- and AERONET-derived AOD values indicate that modelled AODs are overestimated by ~ 20 - 30%. Further research into model parameterisation (e.g. injection height) and the aerosol emission factors used is required to investigate this bias, particularly so as it is likely that we underestimate fuel consumption due to SEVIRI MWIR channel saturation during this extreme wildfire event. The European Union (EU) has recently signed a delegation agreement with ECMWF to provide the services implemented in MACC, including the FRP-based Global Fire Assimilation System (GFAS; Kaiser *et al.*, 2012), in an operational manner until at least 2020. This includes on-going developments of GFAS which aim at providing emission estimates with an hourly temporal resolution by combining FRP observations from both polar orbiting and geostationary satellites. Key pre-requisites are the implementation of

a model for the diurnal cycle of FRP (Andela *et al.* 2015) and a suitable bias correction for geostationary FRP products to account for the omission of low intensity fires, building on the simple linear bias corrections applied currently in the FRP-GRID products.

7.0 Acknowledgements

Funding for this work came from the UK NERC National Centre for Earth Observation (NCEO), from the LSA SAF project, from EUMETSAT and the EU H2020 project MACC-III (contract no. 633080). SEVIRI data were kindly provided under an ESA/EUMETSAT AO, the MODIS data were provided by the NASA EDC DAACS and the European Forest Fire Information System (EFFIS; http://effis.jrc.ec.europa.eu) of the European Commission Joint Research Centre provided burned area data. The GOES\SEVIRI WFABBA data were kindly provided by the Cooperative Institute for Meteorological Satellite Studies (CIMSS) within the Space Science and Engineering Center (SSEC) at University of Wisconsin (UW-Madison) as a collaborative effort between NOAA / NESDIS / STAR and UW-CIMSS personnel. The SEVIRI FRP product were provided by the LSA SAF (http://landsaf.meteo.pt/), the FDeM product was provided by Carlos C. DaCamara and Sofia Ermida at Universidade de Lisboa (http://www.fc.ul.pt/). The FIR fire products were obtained from EUMETSAT EO portal (https://eoportal.eumetsat.int/). The authors would also like to thank Allessio Lattanzio (EUMETSAT), Isabel Trigo (LSASAF) and Yves Govaerts (Rayference) for the assistance and advice provided during this study.

8.0 References

Amraoui, M., DaCamara, C. C. and Pereira, J. M. C. (2010) Detection and monitoring of African vegetation fires using MSG-SEVIRI imagery. *Remote Sensing of Environment*. 114. 1038-1052.

Andela, N., Kaiser, J.K, van der Werf, G., Wooster, M.J. (submitted) New fire diurnal cycle characterizations to improve Fire Radiative Energy assessments made from low-Earth orbit satellites sampling, *Atmos. Chem. Phys*., 15(15):8831–8846.

Baldassarre, G., Pozzoli, L., Schmidt, C. C., Unal, A., Kindap, T., Menzel, W. P., Whitburn, S., Coheur, P.-F., Kavgaci, A., and Kaiser, J. W. (2015). Using SEVIRI fire observations to drive smoke plumes in the CMAQ air quality model: a case study over Antalya in 2008. *Atmospheric Chemistry and Physics*, 15(14):8539–8558.

Andreae, M. O., and P. Merlet (2001) Emission of trace gases and aerosols from biomass burning. *Global Biogeochemical Cycles,* 15. 4. 995-966.

Berk, A., Anderson, G.P., Acharya, P.K., Bernstein, L.S., Muratov, L., Lee, J., Fox, M., Adler-Golden, S.M., Chetwynd, J.H., Hoke, M.L., Lockwood, R.B., Gardner, J.A., Cooley, T.W., Borel, C.C., & Lewis, P.E. (2005). MODTRAN (TM) 5, a reformulated atmospheric band model with auxiliary species and practical multiple scattering options: Update. *Algorithms and Technologies for Multispectral, Hyperspectral, and Ultraspectral Imagery XI, 5806*, 662-667

Calle, A., Casanova, J-L. and Gonzales-Alonso, F. (2009) Impact of point spread function of MSG SEVIRI on active fire detections. *International Journal of Remote Sensing*. 30. 17. 4567-4579.

Center for International Earth Science Information Network (CIESIN) and Centro Internacional de Agricultura Tropical (CIAT) Gridded Population of the World Version 3 (GPWv3). Palisades, NY. CIESIN Columbia University. http://sedac.ciesin.columbia.edu/gpw/index.jsp. (last access : 10/11/2015)

Chen, Y., Li, Q., Randerson, J. T., Lyons, E. A., Kahn, R. A., Nelson, D. L. and Diner, D. J. (2009) The sensitivity of CO and aerosol transport to the temporal and vertical distribution of North American boreal fire emissions. *Atmospheric Chemistry and Physics*. 9. 6559-6580.

Csiszar, I., Schroeder, W., Giglio, L., Ellicott, E., Vadrevu, K. P., Justice, C. O. and Wind, B. (2014) Active fires from Suomi NPP Visible Infrared Imaging Radiometer Suite : Product status and fire evaluation results. *Journal of Geophysical Research : Atmospheres*. 119. 2. 803-816.

Derrien, M. and Le Gleau, H. (2005) MSG/SEVIRI cloud mask and type from SAFNWC. *International Journal of Remote Sensing*. 26. 21. 4707-4732.

Deneke, H.M., & Roebeling, R.A. (2010). Downscaling of METEOSAT SEVIRI 0.6 and 0.8 mu m channel radiances utilizing the high-resolution visible channel. *Atmospheric Chemistry and Physics, 10*, 9761-9772

Dirksen, R. J,, Boersma, K. F,, de Laat, J, Stammes, P., van der Werf, G. R., Martin, M. V., and Kelder, H. M., (2009) An aerosol boomerang: rapid around-the-world transport of smoke from the December 2006 Australian forest fires observed from space. *Journal of Geophysical Research.* 114. D2116. doi:10.1029/2009JD012360

Dozier, J., (1981) A method for satellite identification of surface temperature fields of sub-pixel resolution. *Remote Sensing of Environment*. 11. 221-229.

1264 Ellicott, E., Vermote, E., Giglio, L., and Roberts, G (2009) Estimating biomass consumed
1265 from fire using MODIS FRE. *Geophysical Research Letters*. 36. L13401,
1266 doi:10.1029/2009GL038581.
1267
1268 EUMETSAT (2007) Active Fire Monitoring with MSG. *Algorithm Theoretical Basis*
1269 *Document*. EUM/MET/REP/07/0170. Darmstadt. Germany.
1270
1271 European Commission (2010) Forest Fires in Europe 2009. EUR 24502 EN. Office for
1272 Official Publications of the European Communities. Luxembourg. p. 81.
1273
1274 Freeborn, P. H., Wooster, M. J., Hao, W. M., Ryan, C. A., Nordgren, B. L, Baker, S. P. and
1275 Ichoku, C. (2008) Relationships between energy release, fuel mass loss, and trace gas and
1276 aerosol emissions during laboratory biomass fires. *Journal of Geophysical Research*. 113.
1277 D01301. doi:10.1029/2007JD008679
1278
1279 Freeborn, P. H., Wooster, M. J., Roberts, G., Malamud, B. D. and Xu, W. (2009)
1280 Development of a virtual active fire product for Africa through a synthesis of geostationary
1281 and polar orbiting satellite data. *Remote Sensing of Environment*. 113. 1700-1711.
1282
1283 Freeborn, P. H., Wooster, M. J., Roberts, G. (2011) Addressing the spatiotemporal sampling
1284 design of MODIS to provide estimates of the fire radiative energy emitted from Africa.
1285 *Remote Sensing of Environment*. 115. 2. 475 – 489
1286
1287 Freeborn, P. H., Wooster, M. J., Roberts, G. and Xu, W. (2014a) Evaluating the SEVIRI Fire
1288 Thermal Anomaly Detection Algorithm across the Central African Republic Using the
1289 MODIS Active Fire Product. *Remote Sensing*. 6. 1890-1917. Doi:10.3390/rs6031890.
1290
1291 Freeborn, P. H., Cochrane, M. A. and Wooster, M. J. (2014b) A decade long, multi-scale map
1292 comparison of fire regime parameters derived from three publically available satellite-based
1293 fire products : a case study in the Central African Republic. *Remote Sensing*. 6. 5. 4061-4089.
1294
1295 Freeborn, P.H., Wooster, M.J., Roy, D.P., & Cochrane, M.A. (2014c). Quantification of
1296 MODIS fire radiative power (FRP) measurement uncertainty for use in satellite- based active

fire characterization and biomass burning estimation. *Geophysical Research Letters, 41*, 1988-1994

Fromm, M., Jerome, A., Hoppel, K., Hornstein, J., Bevilacqua, R., Shettle, E., Servranckx, R., Zhanqing, L., and Stocks, B. (2000) Observations of boreal forest fire smoke in the stratosphere by POAM III, SAGE II, and lidar in 1998. *Geophysical Research Letters*. 27. 1407–1410. doi:10.1029/1999GL011200.

Garcia-Meenedez, F., Hu, Y. and Odman, M. T. (2014) Simulating smoke transport from wildland fires with a regional-scale air quality model : Sensitivity to spatiotemporal allocation of fire emissions. *Science of the Total Environment*. 493. 544-553.

Georgiev, C.G., Stoyanova, J.S. (2013) Parallel use of SEVIRI LSA SAF FRP and MPEF FIR products for fire detection and monitoring. *2013 EUMETSAT Meteorological Satellite Conference. 19th American Meteorological Society. AMS Satellite Meteorology, Oceanography and Climatology Conference.* 16th-20th September. 2013. Vienna. Austria. ISSN 1011-3932

Giglio, L., Descloitres, J., Justice, C. O., and Kaufman, Y. J., (2003) An enhanced contextural fire detection algorithm for MODIS. *Remote Sensing of Environment*. 87. 2-3. 273-282.

Gitas, I. Z., Polychronaki, A., Katagis, T and Mallinis, G. (2008) Contribution of remote sensing to disaster management activities : A case study of the large fires in the Peloponnese, Greece. *International Journal of Remote Sensing*. 29. 6. 1847-1853. Doi: 10.1080/01431160701874553

Govaerts, Y., (2006) RTMOM V0B.10 Evaluation report, report EUM/MET/DOC/06/0502, EUMETSAT. 2006. 2226.

Guan, H., Chatfield, R., B., Freitas, S. R., Bergstrom, R. W., Longo, K. M. (2008) Modeling the effect of plume-rise on the transport of carbon monoxide over Africa with NCAR CAM. *Atmospheric Chemistry and Physics*. 8. 6801–6812.

Holben, B. N., Smirnov, A., Eck, T. F., Slutsker, I., Abuhassan, N., Newcomb, W. W., Schafer, J. S., Tanre, D., Chatenet, B., and Lavenu, F. (2001) An emerging ground-based aerosol climatology: Aerosol optical depth from AERONET. *Journal of Geophysical Research: Atmospheres*. 106. 12 067–12 097. doi: 10.1029/2001JD900014

Hollingsworth, A., Engelen, R. J., Benedetti, A., Dethof, A., Flemming, J., Kaiser, J. W., Morcrette, J-J., Simmons, A. J., Textor, C., Boucher, O., Chevallier, F. Rayner, P., Elbern, H., Eskes, H., Granier, C., Peuch, V-H., Rouil, L., and Schultz, M. G. (2008) Toward a Monitoring and Forecasting System For Atmospheric Composition: The GEMS Project. *Bulletin of the American Meteorological Society.* 89. 1147–1164. doi: http://dx.doi.org/10.1175/2008BAMS2355.1

Ichoku, C. and Kaufman, Y. J. (2005) A method to derive smoke emission rates from MODIS fire radiative energy measurements, *IEEE Transactions on Geoscience and Remote Sensing*. 43. 2636–2649.

Jacobson, M. Z. (2014) Effects of biomass burning on climate, accounting for heat and moisture fluxes, black and brown carbon, and cloud absorption effects. *Journal of Geophysical Research : Atmospheres*. 119. 8980-9002. Doi:10.1002/2014JD021861.

Jenkins, B. M., Baxter, L. L., Miles Jr, T. R., and Miles, T. R. (1998) Combustion properties of biomass. *Fuel Processing Technology*. 54. 17 – 46.

Joro, S., Samain, O., Yildirim, A., van de Berg, L. and Lutz, H. J. (2008) Towards an improved active fire monitoring product for MSG satellites. www.eumetsat.int/cs/idcplg?IdcService=GET_FILE&dDocName=pdf_conf_p_s8_47_joro_v&allowInterrupt=1&noSaveAs=1&RevisionSelectionMethod=LatestReleased

Justice, C. O., Vermote, E., Townshend, J. R. G., DeFries, R., Roy, D. P., Hall, D. K., Salomonson, V. V., Privette, J. L., Riggs, G., Strahler, A., Lucht, W., Myneni, R. B., Knyazikhin, Y., Running, S. W., Nemani, R. R., Wan, Z., Huete, A. R., van Leewen, W., Wolfe, R. E., Giglio, L., Muller, J-P., Lewis, P., and Barnesly, M. J. (1998) The Moderate

Resolution Imaging Spectrometer (MODIS) : Land Remote Sensing for Global Change Research. *IEEE Transactions on Geoscience and Remote Sensing*. 36. 4. 1228-1249

Kaiser. J. W., Heil, A., Andrae, M. O., Benedettie, A., Chubarova, N., Jones, L., Morcrette, J-J., Razinger, M., Schultz, M. G., Suttie, M. and van der Werf, G., R. (2012) Biomass burning emissions estimates with a global fire assimilation system based on observed fire radiative power. *Biogeosciences*. 9. 5125-5142. doi:10.5194/bg-9-5125-2012

Kaiser, J. W., Suttie, M., Flemming, J., Morcrette, J.-J., Boucher, O. and Schultz, M. G. (2009a). Global real-time fire emission estimates based on space-borne fire radiative power observations. *AIP Conference Proceedings*, 1100:645–648.

Kaiser, J. W., Boucher, O., Doutriaux-Boucher, M., Flemming, J., Govaerts, Y. M., Gulliver, J., Heil, A., Jones, L., Lattanzio, A., Morcrette, J.-J., Perrone, M. R., Razinger, M., Roberts, G., Schultz, M. G., Simmons, A. J., Suttie, M., and Wooster, M. J. (2009b). Smoke in the air. *ECMWF Newsletter*, 119. 9–15. European Centre for Medium-range Weather Forecasts.

Kaufman, Y. J., Remer, L., Ottmar, R., Ward, D., Rong-R, L., Kleidman, R., Frase, R., Flynn, L., McDougal, D., and Shelton, G. (1996) Relationship between remotely sensed fire intensity and rate of emission of smoke : SCAR-C experiment. In J, Levine (Ed.), Global biomass burning (pp. 685 – 696). MA: MIT Press.

Kaufman, Y. J., Justice, C. O., Flynn, L. P., Kendall, J. D., Prins, E. M., Giglio, L., Ward, D. E., Menzel, W. P., and Setzer, A. W., (1998) Potential global fire monitoring from EOS-MODIS. *Journal of Geophysical Research*. 103. 32215-32238.

Kaufman, Y. J. and Remer, L. A. (1994) Detection of forests using Mid-IR reflectance : An application for aerosol studies. *IEEE Transactions on Geoscience and Remote Sensing*. 32. 3. 672-683.

Koutsias, N., Arianmoutsou, M., Kallimanis, A. S., Mallinis, G., Halley, J. M., and Dimopoulos, P. (2012) Where did the fires burn in Peloponnese, Greece the summer of 2007? Evidence for a synergy of fuel and weather. *Agricultural and Forest Meteorology*. 156. 41-53.

Leung ,F-Y, T., Logan, J. A., Park, R., Hyer, E., Kasischke, E., Streets, D and Yurganov, L. (2007) Impacts of enhanced biomass burning in the boreal forests in 1998 on tropospheric chemistry and the sensitivity of model results to the injection height of emissions. *Journal of Geophysical Research*. 112. D10313, doi:10.1029/2006JD008132

Li, Z, Kaufman, Y. J., Ichoku, C., Fraser, R., Trishchenko, A., Giglio, L. and Yu, X. (2001) A review of AVHRR-based active fire detection algorithms: Principles, limitations, and recommendations. *Global and regional vegetation fire monitoring from space, planning and coordinated international effort*. Academic Publishing. The Hague. 199-225pp

Liu, Y., Kahn, R. A., Chaloulakou, A. and Koutrakis, P. (2009) Analysis of the impact of the forest fires in August 2007 on air quality of Athens using multi-sensor aerosol remote sensing data, meteorology and surface observations. *Atmospheric Environment*. 43. 3310-3318.

Marlier, M.E., Voulgarakis, A., Shindell, D.T., Faluvegi, G., Henry, C.L. and Randerson, J.T. (2014) The role of temporal evolution in modeling atmospheric emissions from tropical fires. *Atmospheric Environment.* 89. 158-168. doi:10.1016/j.atmosenv.2014.02.039.

Matson, M. (1981) Identification of subresolution high temperature sources using a thermal IR sensor. *Photogrammetric Engineering and Remote Sensing* 47, 1311-1318.

Mistakis, E, Stamos, I., Panakinolaou, A., Aifadopoulou, G. and Kontoes, H (2014) Assessment of extreme weather events on transport networks : case study of the 2007 wildfires in Peloponnesus. *Natural Hazards*. 72. 87-107. Doi:10.1007/s11069-013-0896-3.

Mitsopoulos, I. D. and Dimitrakopoulos, A. P. (2013) Estimation of canopy fuel characteristics of Aleppo pine (Pinus halepensis Mill.) forests in Greece based on common stand parameters. *European Journal of Forest Research*. 133:73-79, Doi:10.1007/s10342-013-0740-z.

Morcrette, J.-J., L. Jones, J.W. Kaiser, A. Benedetti, O. Boucher (2008) Toward a forecast of aerosols with the ECMWF Integrated Forecast System. *ECMWF Newsletter*. No. 114. ECMWF. Reading. UK

Mu, M., Randerson, J. T., van der Werf, G. R., Giglio, L., Kasibhatla, P., Morton, D., Collatz, G. J., DeFries, R. S., Hyer, E. J., Prins, E. M., Griffith, D. W. T., Wunch, D., Toon, G. C., Sherlock, V., and Wennberg, P. O. (2011) Daily and 3-hourly variability in global fire emissions and consequences for atmospheric model predictions of carbon monoxide. *Journal of Geophysical Research : Atmospheres*. 116. D24303. Doi:10.1029/2011JD016245.

Paugam, R., Wooster, M., Freitas, S. R. and Val Martin, M. (2015a) A review of approaches to estimate wildfire plume injection height within large scale atmospheric chemical transport models – Part 1. *Atmospheric Chemistry and Physics Discuss*ions. 15. 9767-9813.

Paugam, R., Wooster, M., Atherton, J., Freitas, S. R., Schultz, M. G. and Kaiser, J. W. (2015b) Development and optimization of a wildfire plume rise model based on remote sensing data inputs – Part 2. *Atmospheric Chemistry and Physics Discuss*ions. 15. 9815-9895.

Petrenko, M., Kahn, R., Chin, M., Soja, A., Kucsera, T., and Harshvardhan (2012). The use of satellite-measured aerosol optical depth to constrain biomass burning emissions source strength in the global model GOCART. *Journal of Geophysical Research*. 117(D18):D22204. doi:10.1029/2012JD017870

Pereira, G., Shimabukuro, Y. E., Moraes, E. C., Freitas, S. R., Cardozo, F., S., and Longo, K. M. (2011) Monitoring the transport of biomass burning emission in South America. *Atmospheric Pollution Research*. 3. 247-254.

Petitcolin, F. and Vermote, E. (2002) Land surface reflectance, emissivity and temperature from MODIS middle and thermal infrared data. *Remote Sensing of Environment*. 82. 112-134.

Prins, E. M., and Menzel, W. P., (1994) Trends in South American biomass burning with the GOES visible infrared spin scan radiometer atmospheric sounder from 1983 to 1991. *Journal of Geophysical Research*. 99. 16719-16735.

Prins, E. M., Felts, J. M., Menzel, W. P., Ward, D. E. (1998) An overview of GOES-8 diurnal fire and smoke results for SCAR-B and 1995 fire season in South America. *Journal of Geophysical Research*. 103. 31821-31835.

Poupkou, A., Markakis, K., N..Liora, Giannaros, T. M., Zanis, P., Im, U., Daskalakis, N., Myriokefalitakis, S., Kaiser, J. W., Melas, D., Kanakidou, M., Karacostas, T., and Zerefos, C. (2014). A modeling study of the impact of the 2007 Greek forest fires on the gaseous pollutant levels in the Eastern Mediterranean. *Atmospheric Environment.* 148. 1–17.

Reid, J. S., Prins, E. M., Westphal, D. L., Schmidt, C. C., Richardson, K. A., Christopher, S. A., Eck, T. F., Reid, E. A., Curtis, C. A., and Hoffman, J. P. (2004) Real-time monitoring of South American smoke particle emissions and transport using a coupled remote sensing/box-model approach. *Geophysical Research Letters*. 31. doi:10.1029/2003GL018845.

Reid, J. S., Hyer, E. J., Prins, E. M., Westphal, D. L., Zhang, J., Wang, J., Christopher, S. A., Curtis, C. A., Schmidt, C. C., Eleuterio, D. P., Richardson, K. A. and Hoffman, J. P. (2009) Global monitoring and forecasting of biomass-burning smoke : description of and lessons from the Fire Locating and Modeling of Burning Emissions (FLAMBE) program. *IEEE Journal of Selected Topics in Applied Earth Observations and Remote Sensing*. 2. 3. 144 - 162.

Roberts, G., Wooster, M. J., Perry, G. L. W. , Drake, N., Rebelo, L.-M., Dipotso, F. (2005), Retrieval of biomass combustion rates and totals from fire radiative power observations: Application to southern Africa using geostationary SEVIRI imagery, *Journal of Geophysical Research*. 110. D21111. doi:10.1029/2005JD006018.

Roberts, G. and Wooster, M. J. (2007) New perspectives on Africa biomass burning dynamics. EOS. *Transactions American Geophysical Union.* 88. 38. 369-370.

Roberts, G. and Wooster. M., J. (2008) Fire Detection and Fire Characterization over Africa using Meteosat SEVIRI. *IEEE Transactions on Geoscience and Remote Sensing*. 48. 4. 1200-1219

Roberts, G., Wooster, M. J., and Lagoudakis, E. (2009). Annual and diurnal African biomass burning temporal dynamics. *Biogeosciences*, 6, 849-866.

Roberts, G., Wooster, M. J., Freeborn, P. H. and Xu, W. (2011) Integration of geostationary FRP and polar-orbiting burned area datasets for an enhanced emissions inventory. *Remote Sensing of Environment.* 115. 2047-2061. doi:10.1016/j.rse.2011.04.006

Roberts, G and Wooster, M. J. (2014) Development of a multi-temporal Kalman filter approach to geostationary active fire detection and fire radiative power (FRP) estimation. *Remote Sensing of Environment*. 152. 392-412. DOI: 10.1016/j.rse.2014.06.020

Roy, D. P., Jin, Y., Lewis, P. E. and Justice, C. O. (2005) Prototyping a global algorithm for systematic fire-affected area mapping using MODIS time series data. *Remote Sensing of Environment*. 97. 137 – 162.

Schroeder, W., Prins, E., Giglio, L., Csiszar, I., Schmidt, C., Morisette, J and Morton, D. (2008) Validation of GOES and MODIS active fire detection products using ASTER and ETM+ data. *Remote Sensing of Environment*. 112. 2711-2726.

Schroeder, W., Oliva, P., Giglio, L., Csiszar, I. A. (2014). The New VIIRS 375 m active fire detection data product: Algorithm description and initial assessment. *Remote Sensing of Environment*, 143, 85-96.

Seiler, W., and Crutzen, P. J. (1980). Estimates of gross and net fluxes of carbon between the biosphere and the atmosphere from biomass burning. *Climatic Change*, 2(3), 207-247.

Sofiev, M., Vankevich, R., Lotjonen, M., Prank, M., Petukhov, V., Ermakova, T., Koskinen, J., and Kukkonen, J. (2009) An operational system for the assimilation of the satellite information on wild-land fires for needs of air quality modelling and forecasting. *Atmospheric Chemistry and Physics*. 9. 6833 – 6847.

Sofiev, M., Ermakova, T., and Vankevich, R. (2012) Evaluation of the smoke-injection height from wild-land fires using remote sensing data. *Atmospheric Chemistry and Physics*. 12. 1995-2006. doi:10.5194/acp-12-1995-2012.

Tjemkes, S. A., and Scmetz, J. (1997) Synthetic satellite radiances using the radiance sampling method. *Journal of Geophysical Research*. 102. 1807 – 1818

Theoharatos, G., Pantavou, K., Mavrakis, A., Spanou, A., Katavoutas, G., Efstathiou, P., Mpekas, P., and Asimakopoulos, D (2010) Heat waves observed in 2007 in Athens, Greece: Synoptic conditions, bioclimatological assessment, air quality levels and health effects. *Environmental Research*. 110. 152–161.

Tsyro, S., Simpson, D., Tarrason, L., Klimont, Z., Kupianen, K., Pio, C. and Yttri, K. E. (2007) Modeling of elemental carbon over Europe. Journal of Geophysical Research : Atmospheres. 112. D23S19. 16. DOI: 10.1029/2006JD008164

Turquety, S., Hurtmans, D., Hadji-Lazaro, J., Coheur, P., Clerbaux, C., Josset, D. and Tsamalis, C. (2009) Tracking the emission and transport of pollution from wildfires using the IASI CO retrievals: analysis of the summer 2007 Greek fires. *Atmospheric Chemistry Physics*. 9. 4897–4913.

Turquety, S., Menut, L., Bessagnet, B., Anav, A., Viovy, N., Maignan, F., & Wooster, M. (2014). APIFLAME v1.0: high resolution fire emission model and application to the Euro-Mediterranean region. *Geoscientific Model Development.* 7, 587-612, doi:10.5194/gmd-7-587-2014.

Val Martin, M., Logan, J. A., Kahn, R. A., Leung, F-Y., Nelson, D. L., and Diner, D. J. (2010) Smoke injection heights from fires in North America : analysis of 5 years of satellite observations. *Atmospheric Chemistry and Physics*. 10. 1491-1510.

Vermote, E., Ellicott, E., Dubovik, O., Lapyonok, T., Chin, M., Giglio, G. and Roberts, G. (2009) An approach to estimate global biomass burning emissions of Organic and Black Carbon from MODIS Fire Radiative Power. *Journal of Geophysical Research*. 114. D18205. doi:10.1029/2008JD011188.

van der Werf, G. R., Randerson, J. T., Giglio, L., Collatz, G. J., Mu, M., Kasib- hatla, P. S., Morton, D. C., DeFries, R. S., Jin, Y., and van Leeuwen, T. T. (2010). Global fire emissions and the contribution of deforestation, savanna, forest, agricultural, and peat fires (1997–2009). *Atmospheric Chemistry Phys*ics. 10. 11707–11735.

van der Werf, G. R., Randerson, J. T., Giglio, L., COllatz, G. J., Kasibhatla, P. S. and Arellano Jr, A. F. (2006) Interannual variability of global biomass burning emissions from 1997-2004. *Atmospheric Chemistry and Physics*. 6. 3423-3441.

Veraverbeke, S., Lhermitte, S., Verstraeten, W. W. and Goossens, R. (2010) The temporal dimension of differenced Normalised Burn Ratio (dNBR) fire/burn severity studies : The case of the large 2007 Peloponnese wildfires in Greece. *Remote Sensing of Environment*. 114. 11. 2548-2563. Doi: 10.1016/j.rse.2010.05.029

Verroios, G and Georgiadis, T. (2011) Aleppo pine forests of northern and western Peloponnisos (southern Greece) : Plant communities and diversity. *Plant Biosystems*. 145. 3. 606-619.

World Health Organisation (2006) Air quality guidelines for particulate matter, ozone, nitrogen dioxide and sulphur dioxide. WHO/SDE/PHE/OEH/06.02. *World Health Organization*. WHO Press. Geneva. Switzerland

Wooster, M. J., Zhukov, B., and Oertel, D., (2003) Fire radiative energy for quantitative study of biomass burning: derivation from the BIRD experimental satellite and comparison to MODIS fire products. *Remote Sensing of Environment*. 86. 83-107.

Wooster, M. J., Roberts, G., Perry, G. L. W. and Kaufman, Y. J. (2005) Retrieval of biomass combustion rates and totals from fire radiative power observations: FRP derivation and calibration relationships between biomass consumption and fire radiative energy release. Journal of Geophysical Research. 110, D24311. doi:10.1029/2005JD006318

Wooster, M. J., Xu, W., and Nightingale, T (2012) Sentinel-3 SLSTR active fire detection and FRP product: Pre-launch algorithm development and performance evaluation using MODIS and ASTER datasets. *Remote Sensing of Environment.* 120. 236–254.

Xu, W., Wooster, M. J., Roberts, G. and Freeborn, P. (2010) New GOES imager algorithms for cloud and active fire detection and fire radiative power assessment across North, South and Central America. *Remote Sensing of Environment*. 114. 9. 1876-1895.

Yang, E.-S., Christopher, S. A., Kondragunta, S., and Zhang, X (2011) Use of hourly Geostationary Operational Environmental Satellite (GOES) fire emissions in a Community Multiscale Air Quality (CMAQ) model for improving surface particulate matter predictions. *Journal of Geophysical Research : Atmospheres*. 116. D04303. Doi: 10.1029/2010JD014482.

Zhang, X., Kondragunta, S., Ram, J., Schmidt, C. and Hung, H-C. (2012) Near-real-time global biomass burning emissions product from geostationary satellite constellation. *Journal of Geophysical Research : Atmospheres*. 117. D14201. doi:10.1029/2012JD017459.

Zhukov, B., Lorenz, E., Oertel, D., Wooster, M. and Roberts, G. (2006) Spaceborne detection and characterisation of fires during the bi-spectral infrared detection (BIRD) experimental small satellite mission (2001-2004). *Remote Sensing of Environment*. 100. 29-51. doi:10.1016/j.rse.2005.09.019

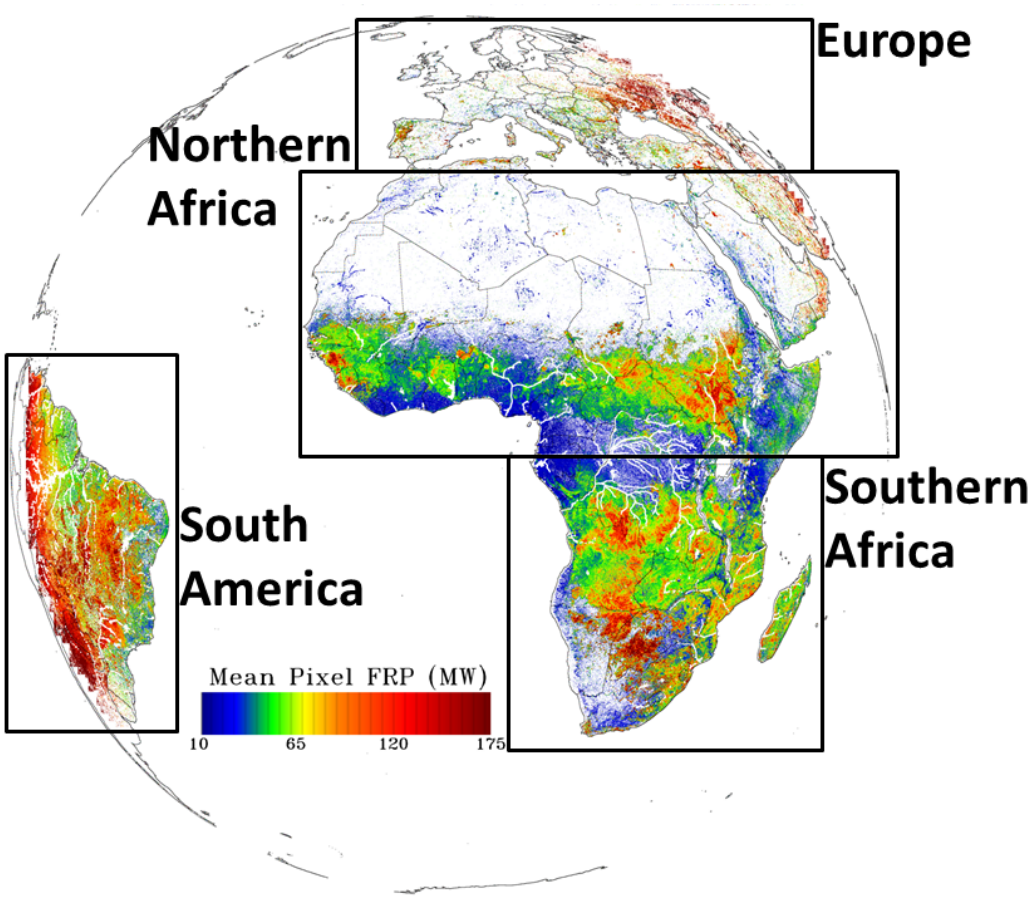

Figure 1: SEVIRI's imaging disk showing the mean per-pixel FRP (MW) seen in each SEVIRI pixel, calculated using all FRP-PIXEL products available between 2008-2013. Also indicated are the four geographic regions that LSA-SAF SEVIRI products are subset to.

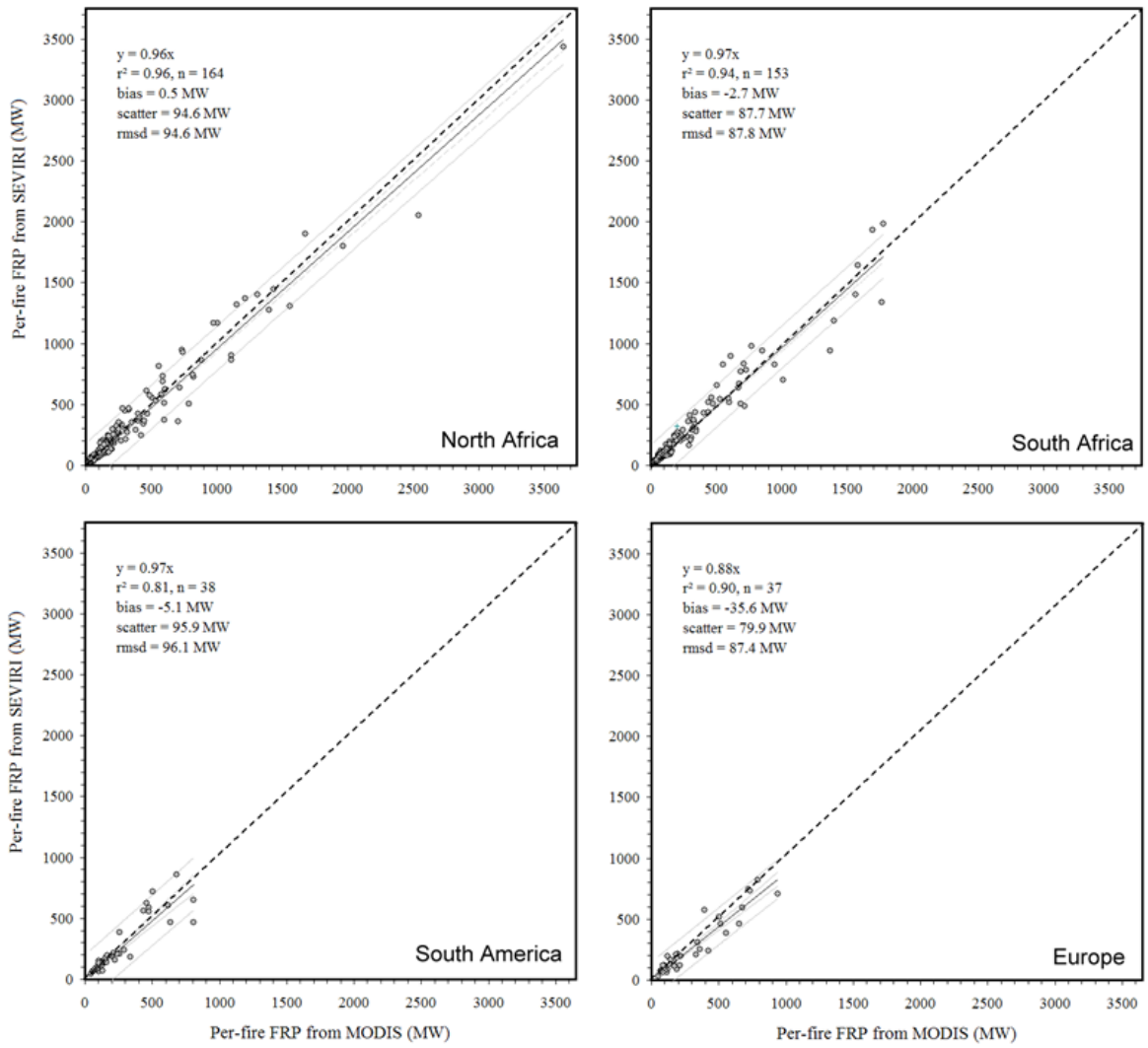

Figure 2: A comparison of per-fire FRP derived from SEVIRI and MODIS observations of fires observed near-simultaneously by each sensor during one week in each LSA SAF geographic region (Figure 1). Fires are designated as contiguous clusters of active fire pixels. SEVIRI FRP were taken from the LSA SAF FRP-PIXEL product in each case and MODIS FRP is taken from the MOD14 product (Collection 5; Giglio *et al.*, 2003). The most radiant fires were detected in the northern Africa region (top left), and all regions are displayed on the same x- and y-axis scales for ease of comparison.

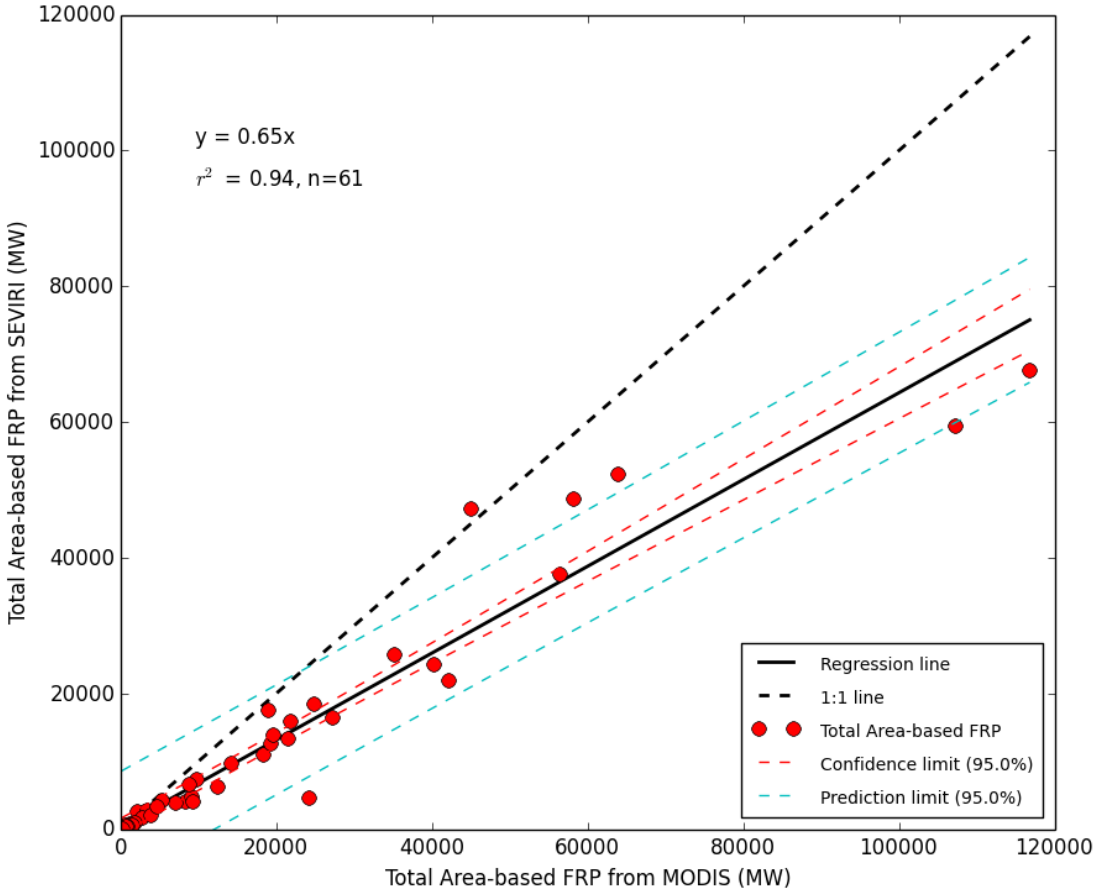

Figure 3: Relationship between regional-scale inter-scene FRP derived from all spatially matched, contemporaneous SEVIRI and MODIS FRP-PIXEL observations for the northern Africa region (1-7 December, 2009). The MODIS swath is taken as the observation area. The least squares linear best-fit passing through the origin is shown (bold line), along with the 95% confidence intervals on the mean (light dotted line) and on the prediction of y from x (outermost lines). The 1:1 line is also shown (dashed). SEVIRI tends to generally underestimate regional-scale FRP, primarily due to the non-detection of the lowest FRP fire pixels, many of which MODIS can detect. However, the degree of underestimation is relatively small as described by the slope of the linear best fit to the data.

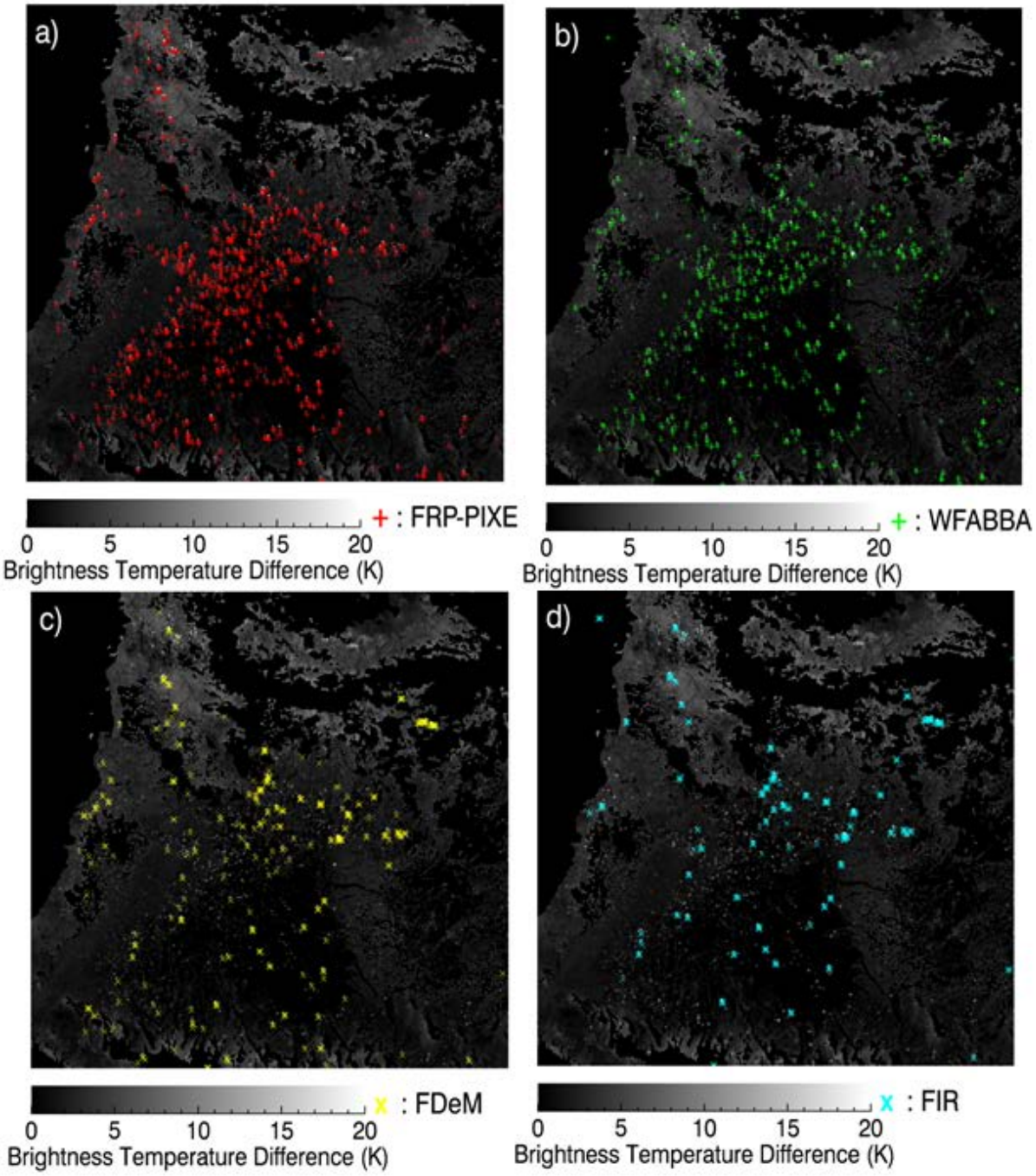

Figure 4 : Example of the active fire pixel detections contained within the four SEVIRI-derived active fire detection products studied herein (LSA SAF FRP-PIXEL product; Wooster *et al.*, 2015, WF-ABBA; Prins *et al.*, 1998, Fire Detection and Monitoring - FDeM; Amraoui *et al.*, 2010, and FIR Active Fire Monitoring; Joro *et al.*, 2008). The images are produced from a single SEVIRI time slot (13:15 UTC on 21st August 2014) and show the active fire detections made in (a) FRP-PIXEL (1249 active fire pixel detections), (b) WFABBA (filtered version; 686 detections made), (c) FDeM (346 detections) and (d) FIR (312 detections). The underlying greyscale image is the SEVIRI brightness temperature difference image (3.9μm - 10.8μm channels) from the same imaging slot. Water bodies and clouds have been masked out (black). The region shown is that over Angola in the southern African LSA SAF geographic region (Figure 1). It is clear than whilst all the products tend to detect a reasonable number of fires that are comprised on multiple SEVIRI active fire pixels,

it is the FRP-PIXEL and WF-ABBA products that detect more of the single pixel fires, with the FRP-PIXEL product dominating in this regard.

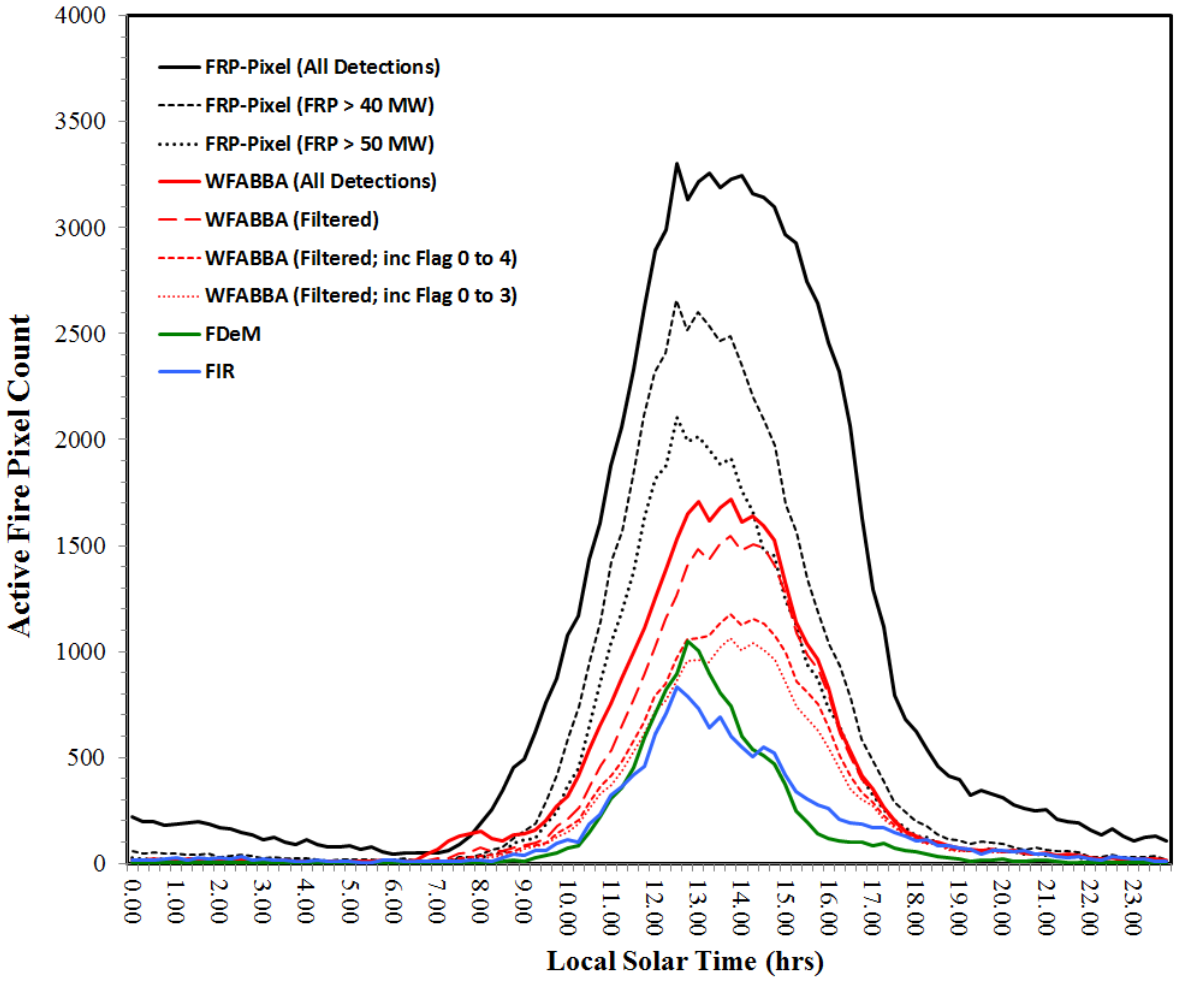

Figure 5: Diurnal cycle of active fire detections present within the four SEVIRI-derived active fire products discussed herein for the LSA SAF southern Africa geographic region (Figure 1) on a single day (30th August 2014). The products are the LSA SAF FRP-PIXEL product (Wooster *et al.*, 2015), Wildfire-ABBA (WFABBA; Prins *et al.*, 1998), Fire Detection and Monitoring (FDeM; Amraoui *et al.*, 2010) and Active Fire Monitoring (FIR; Joro *et al.*, 2008). All confirmed active fire detections made in each product are included here for completeness, and results are shown in terms of the local solar time of detection. For the FRP-PIXEL product, three active fire time-series are shown; 1) all detections, and those only those detections from fire pixels with FRP magnitudes 2) >40 MW and 3) >50 MW since it is known that increasing undercounting of active fire pixels occurs around these limits (Roberts and Wooster, 2008; and companion paper in this issue). For the WFABBA active fire detections, all four versions of the dataset are included 1) all active fire detections, 2) the WFABBA 'filtered' detections where active fire pixels only detected once during 24 hrs are removed; and the WFABBA filtered detections keeping only 3) the high probability fires (flags 0 to 3) and 4) high and medium probability fires (flags 0 to 4). The LSA SAF FRP-PIXEL product detects a total of 89781 active fire pixels over this day, which reduces to 53561 and 39461 when restricted to fire pixels with FRP >40 MW and >50 MW respectively. For WFABBA, the total number of active fire detections is 35759, and the filtered dataset contains 35759 detections which reduces to 30751 and 23957 when WFABBA low and medium probability fire detections are removed. The FDeM and FIR detect only 13477 and 14645 active fire pixels respectively.

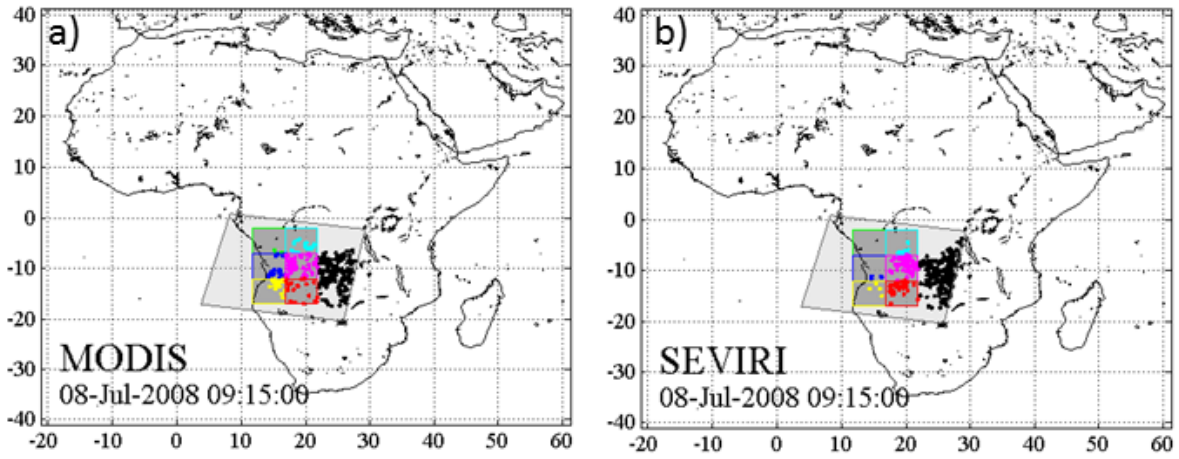

Figure 6: Graphical representation of the procedure used to generate the dataset for use in evaluating the bias adjustment factors used within the FRP-GRID product. Fire pixels were subset from the MOD14 and MYD14 MODIS Active Fire products available between May 2008 and April 2009 using six 5.0° grid cells centred on the MODIS swath, as illustrated in (a). These same grid cells were then used in (b) to subset fire pixels from the SEVIRI full Earth disk images acquired at times coincident with the MODIS overpass, as well as from the three previous SEVIRI imaging timeslots collected prior to the MODIS overpass.

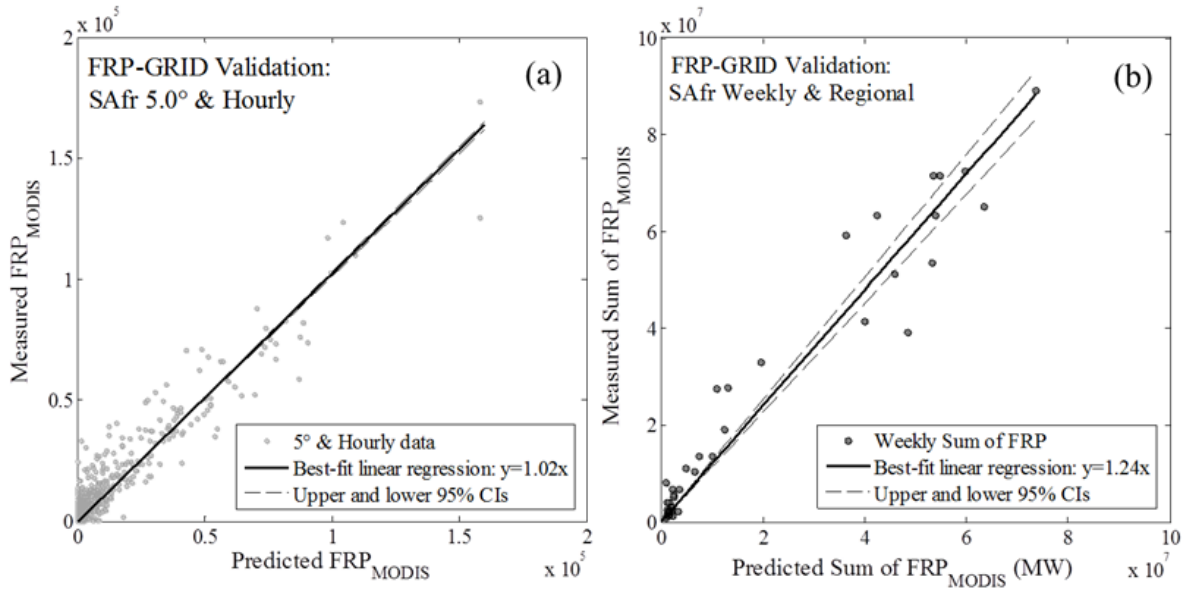

Figure 7: Evaluation of the bias adjustment factors used in the SEVIRI FRP-GRID product. Results are based on coincident SEVIRI and MODIS observations taken between May 2008 and May 2009, collected and matched as shown in Figure 6. The nearly 1:1 relationship between the predicted and measured values of MODIS FRP demonstrates the unbiased nature of the adjustment factor applied at (a) 5.0° grid cell resolution and hourly temporal resolution in the FRP-GRID product, in this case for 5.0° grid cells in southern Africa. In (b) the effect of accumulating observations over weekly intervals and over the entire southern Africa LSA SAF geographic region demonstrates that the FRP-GRID product tends to still deliver a result that underestimates the sum of FRP measured by MODIS at this broader spatiotemporal scale, owing primarily to the numerous observations in which SEVIRI failed to detect at least one active fire pixel in a 5.0° grid cell in which MODIS did successfully detect a fire. Full results of the evaluation exercise for all four geographic regions are presented in Table 3.

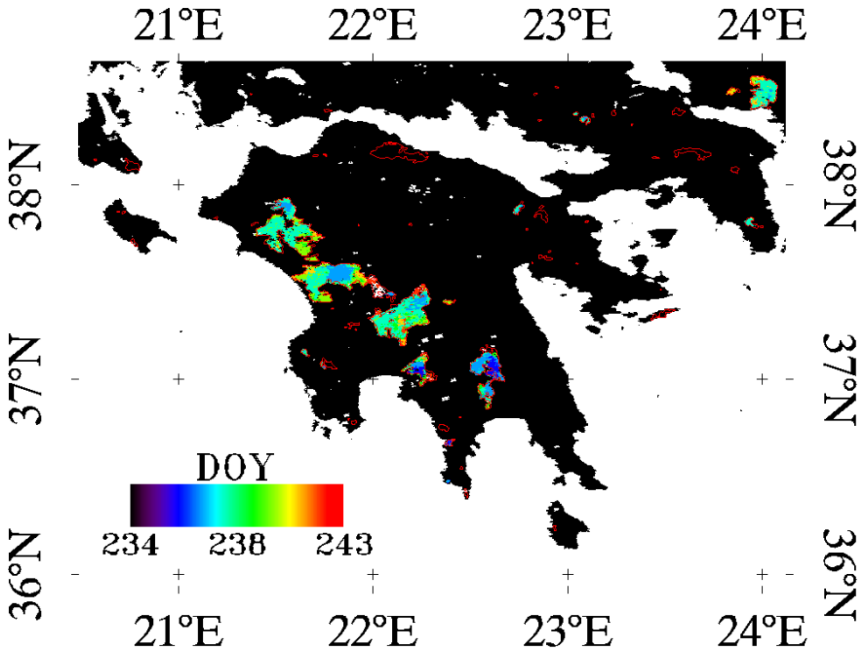

Figure 8: The Peloponnese wildfires as viewed by the MODIS 500m burned area of Roy *et al.* (2005) collected in August and September 2007 and coloured by day of the year they were detected (DOY). The fires occurred in areas forest, shrublands and olive groves and affected 1847 km^2 according to these data. Also shown as a red outline are the 2007 burned area perimeters extracted from the European Forest Fire Information System (EFFIS; European Commission, 2010) that encompass 1628 km^2.

a)

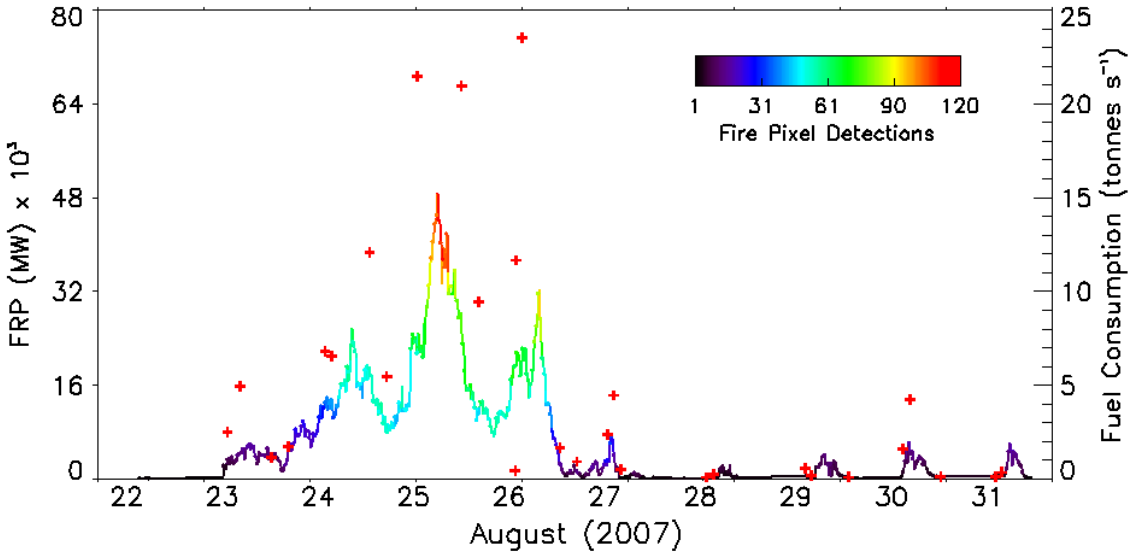

b)

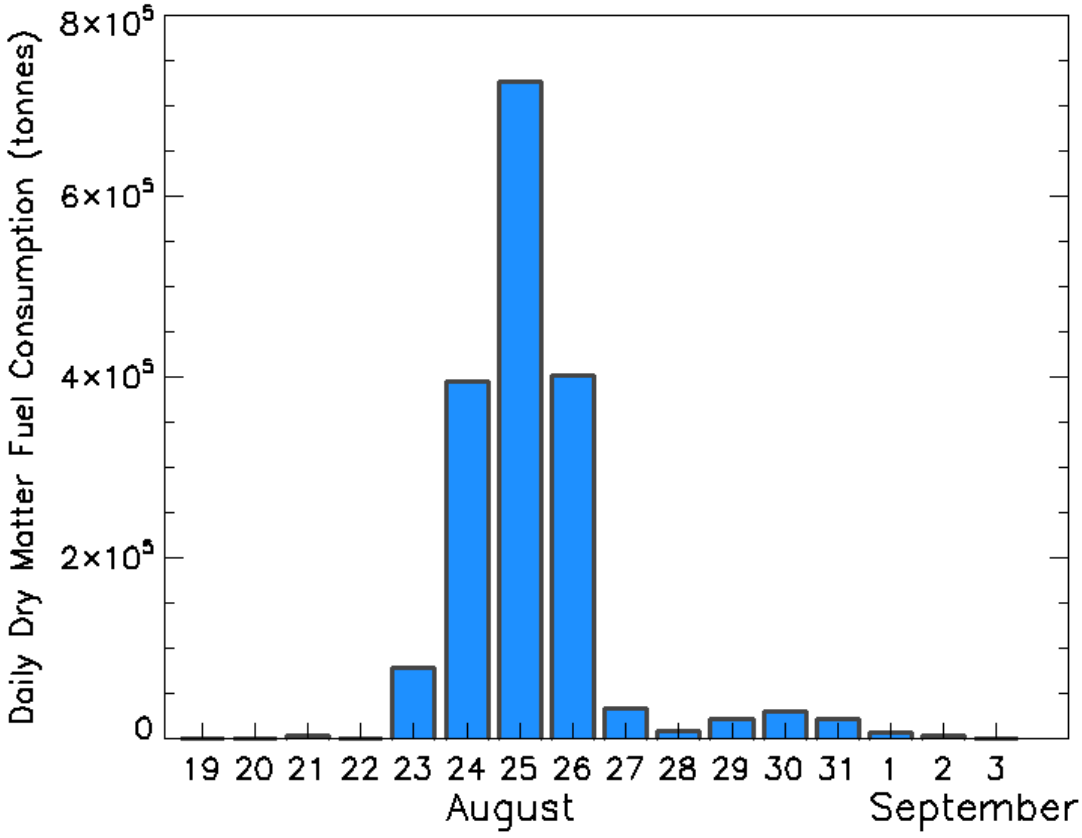

Figure 9: (a) Time series of atmospherically corrected SEVIRI FRP measures (MW, left axis) and equivalent fuel consumption rate (tonnes s^{-1}) for the Peloponnese wildfires, as measured between 22nd and 31st August 2007 using the LSA SAF SEVIRI FRP-PIXEL product. Also shown are the atmospherically corrected MODIS FRP data collected over the same time period (red crosses). Note that for clarity of presentation the MODIS FRP measure recorded on 25th August (12:05 UTC) is not shown as this exceeds 180 GW, and SEVIRI

reaches a far lower value due to strong prevalence of SEVIRI MWIR channel pixel saturation at this time. (b) Daily total dry matter fuel consumption estimated using the time-integrated SEVIRI FRP data. We estimate 1.74Tg of fuel was consumed in these fires, the bulk of which was burned between 24-26th August.

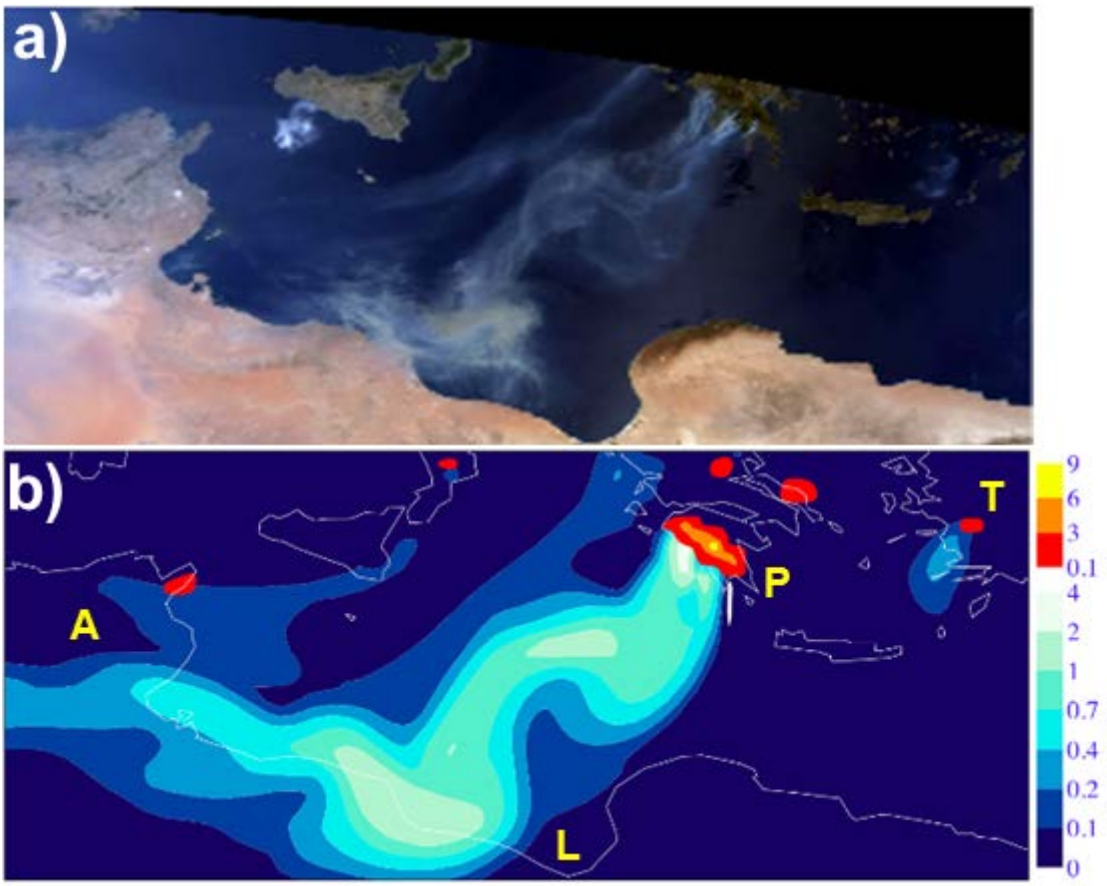

Figure 10: (a) MODIS Terra *'true'* colour composite derived for August 26th (09:35 UTC) and (b) fire-emitted smoke aerosol optical depth at 550 nm derived using the modelling scheme detailed in Section 5.2 (blue scale) along with SEVIRI-derived FRP-density observations derived from the FRP-PIXEL product [W m^2, top, red scale] and interpolated to the atmospheric model grid. The FRP-PIXEL observations indicate the smoke plume sources and highlight the strength of the Peloponnese fires at this time. The Peloponnese (P), Libya (L), Algeria (A) and Turkey (T) are identified. MODIS data source in (a): http://rapidfire.sci.gsfc.nasa.gov.

a) b)

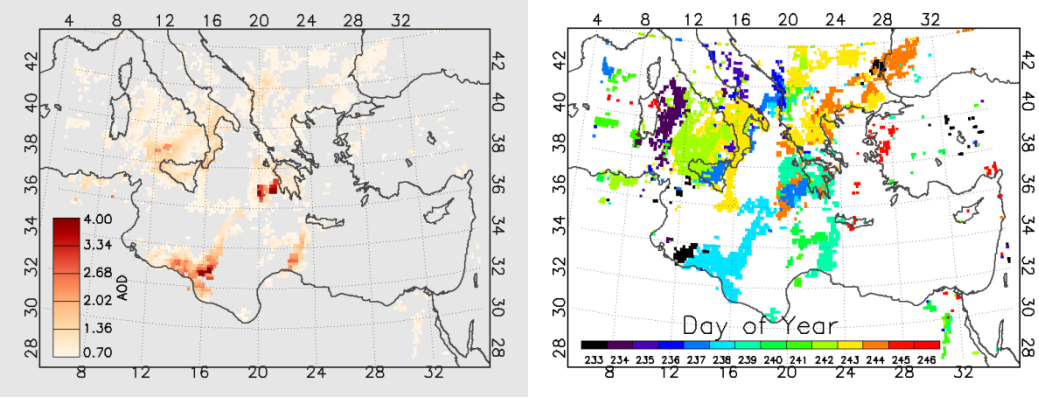

Figure 11 : Data extracted for the 2007 Mediterranean 'mega-fire' event from Terra and Aqua MODIS Aerosol Optical Depth (AOD) products (a) Maximum value composite of atmospheric Aerosol Optical Depth (AOD) developed using Terra and Aqua MODIS observations (MOD04 and MYD04 products) acquired between the 21st August and 3rd September 2007. Only pixels with an AOD value in excess of 0.7 are shown. (b) Day of the year (DOY) of the highest AOD value shown in (a).

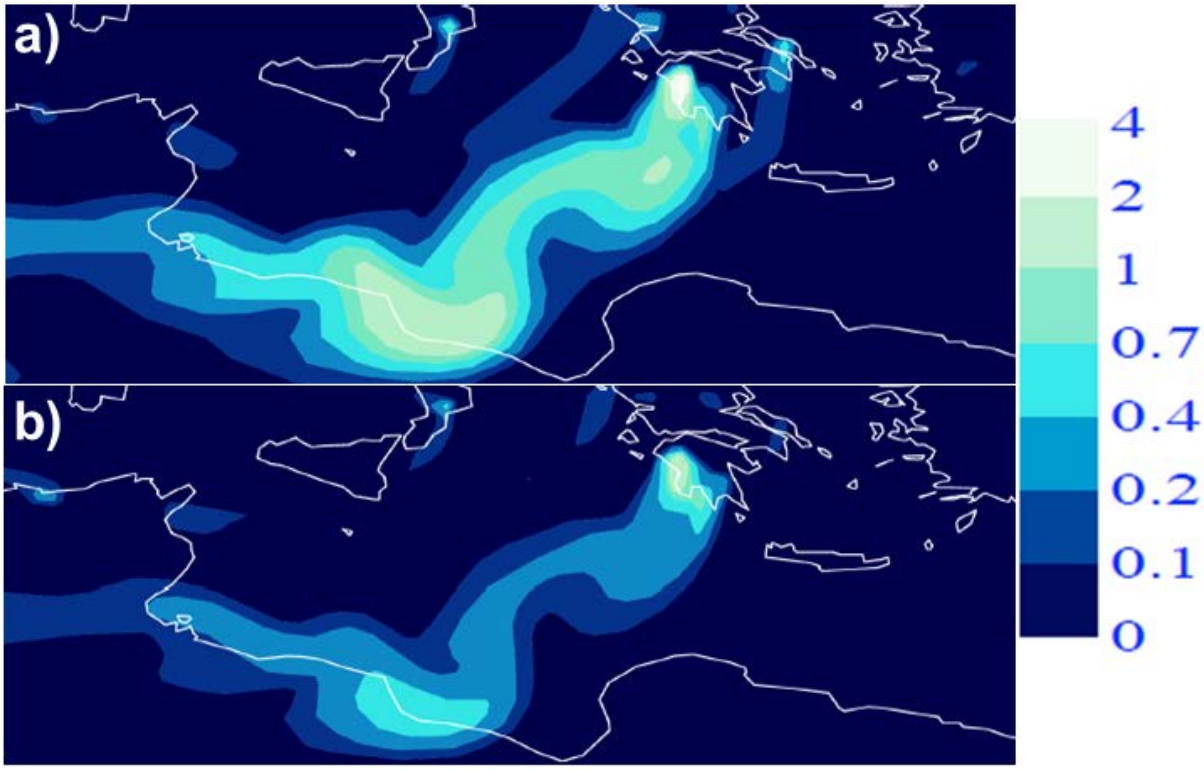

Figure 12: Modelled smoke plume on the 26th August (09:35 UTC) calculated using (a) daily, and (b) weekly temporal resolution FRP-derived smoke source emissions as described in Section 5.4. The blue scale indicates variations in the modelled smoke aerosol optical depth (AOD) at 550nm. The corresponding modelled AOD obtained using hourly FRP-derived source emissions is shown in Figure 10b.

a)

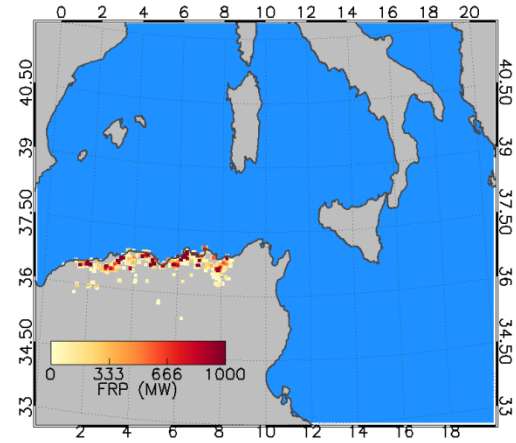

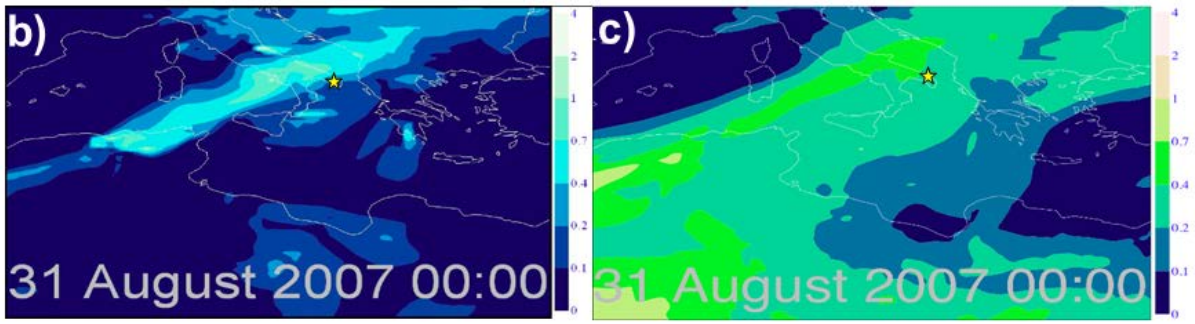

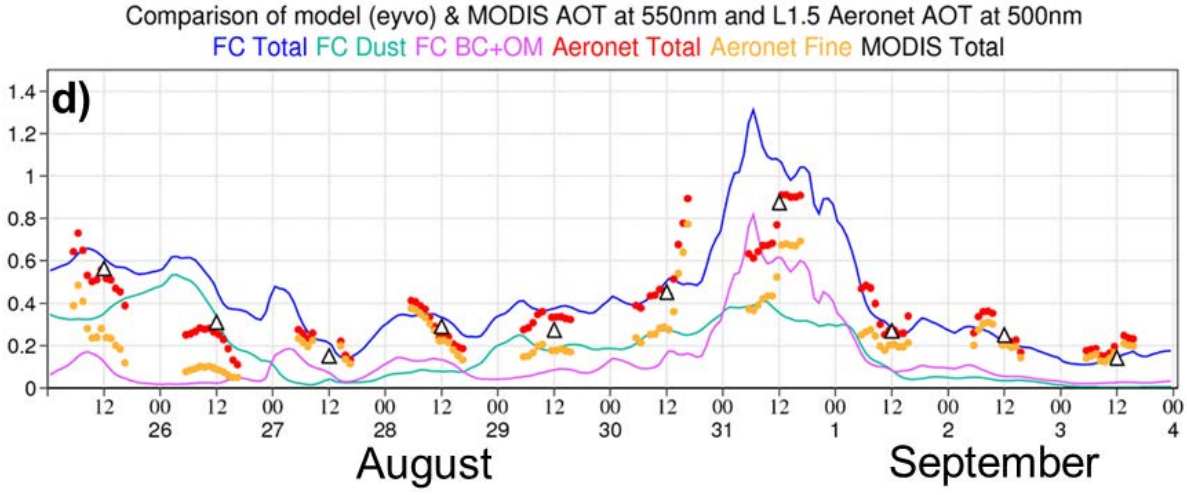

Figure 13: MODIS FRP from the Algerian wildfires (a) between the 26th August and 4th September (2007), (b) modelled smoke, and (c) modelled dust aerosol optical depth (AOD) at 550 nm on August 31st 2007 (00:00 UTC). (d) time series of daily averaged MODIS total AOD observations (open black triangles), the AERONET observations of total (red circles) and fine mode AOD (orange circles), modelled total AOD (blue line), and its contributions due to smoke (purple line) and dust (green line). Data sources: MODIS (http://disc1.sci.gsfc.nasa.gov) and AERONET (http://aeronet.gsfc.nasa.gov)

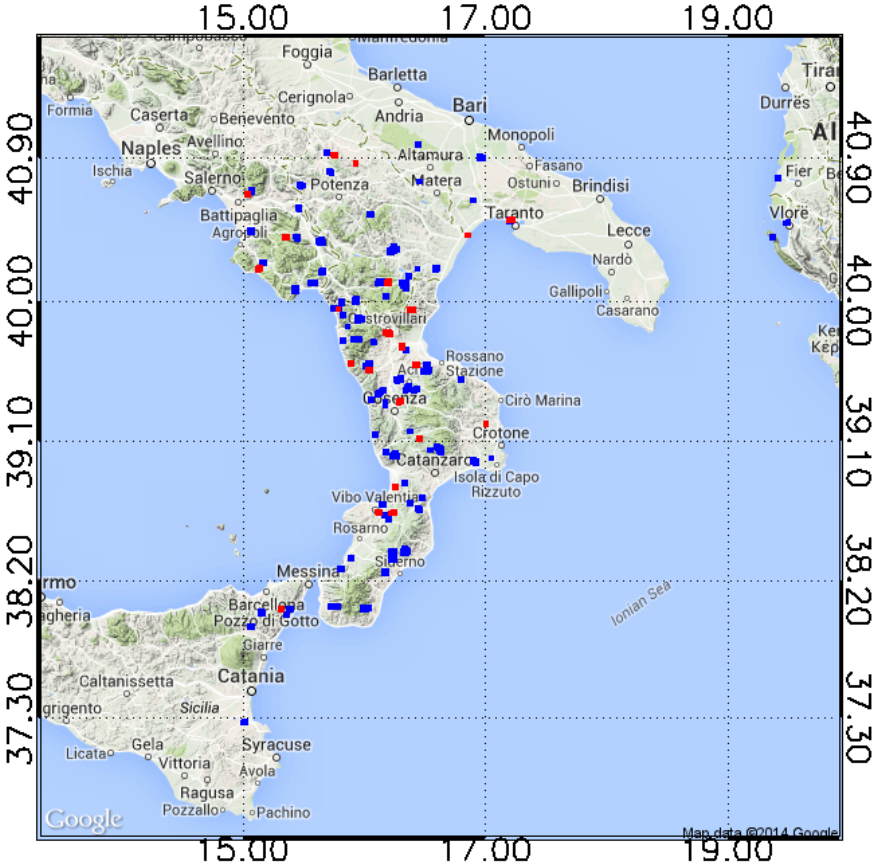

Figure 14 : MODIS active fire detections occurring between the 27 and 31st August (blue symbols) and 28 and 29th August (red symbols). These fires typically occur downwind of the Algerian smoke plume seen in Figure 13, and therefore are likely to have contributed to elevated AOD values detected at the Lecce AERONET site.

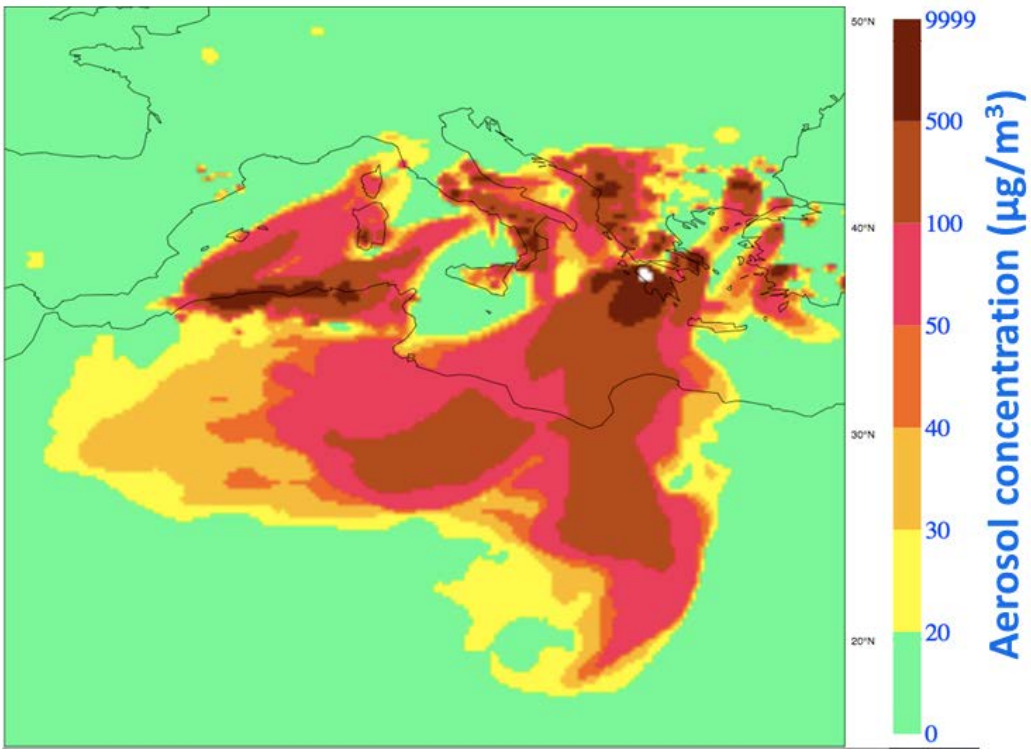

Figure 15: Simulated maximum 24-hour running mean smoke aerosol concentration [µg m^{-3}] recorded at the surface between the 23rd August and 3rd September (2007), based on the methodology outlined in Section 5.6. The values are an upper limit due to unrealistically low smoke injection height into the atmosphere. The World Health Organisation (WHO) air quality guidelines (WHO, 2006) set a limit of 25 µg m^{-3} for the surface concentration of fine mode particulate matter (PM2.5) averaged over a 24 hour period.

Table 1: Performance characteristics of the LSA SAF Meteosat SEVIRI FRP-PIXEL product in the four LSA SAF geographical regions, as compared to MODIS active fire product (Collection 5 MOD14 and MYD14) collected over the same area and at the same time. Errors of omission and commission with respect to MODIS were calculated on a per fire pixel basis as described in Section 3.1.1. The per-fire basis results (Column 5) were obtained when comparing the total FRP retrieved from MODIS and SEVIRI for fires (defined as a spatially contiguous set of active fire pixels) detected by both sensors. The area-based results (column 6) were derived from comparison of the total FRP measured by all detected fires in a matching MODIS and SEVIRI image area, and thus include the influence of non-detected low FRP fires by SEVIRI whilst the per-fire comparison results (Column 5) do not.

LSA SAF Geographic Region	**Image Dates (2008)**	**Active Fire Pixel Detection Omission Error (%)**	**Active Fire Pixel Detection Commission Error (%)**	**Slope of linear best fit relationship between SEVIRI-to-MODIS per-fire-based FRP measures**	**Slope of linear best fit relationship between SEVIRI-to-MODIS Area-based FRP measures**
northern Africa	1-8 Dec	65	9	0.96	0.65
southern Africa	19-24 Aug	77	13	0.97	0.53
South America	14-24 Aug	91	39	0.97	0.22
Europe	9-17 Aug	97	30	0.88	0.11

Table 2 : Summary of active fire pixel detection errors of omission and commission for the four SEVIRI-derived active fire products explored herein (LSA SAF FRP-PIXEL product; Wooster *et al.*, 2015, WF-ABBA; Prins *et al.*, 1998, Fire Detection and Monitoring - FDeM; Amraoui *et al.*, 2010, and FIR Active Fire Monitoring; Joro *et al.*, 2008). Data were collected over the LSA SAF southern Africa geographic region during August 2014, when fire activity is widespread in this area. The MODIS active fire products (MOD14 and MYD14; Giglio *et al.*, 2003) acted as the independent data source for the comparison.

	FRP-PIXEL	**WFABBA**	**WFABBA**	**WFABBA**	**WFABBA**	**FDeM**	**FIR**
		All Detections	**Filtered**	**Filtered (Flags 0-4)**	**Filtered (Flags 0-3)**		
Number of SEVIRI fire pixels at coincident MODIS overpasses	33414	15610	13008	9736	8832	7664	7151
Number of SEVIRI fire pixels detected by MODIS	29037	14521	12284	9369	8496	7260	6730
Commission error (%)	13	7	6	4	4	5	6
Omission error (%)	77	82	84	87	88	92	95

Table 3: Summary of the results related to evaluation of the regional bias adjustment factors implemented during the processing of the LSA SAF FRP-GRID product. Slope of the linear best fit between the SEVIRI-predicted regional FRP using the FRP-GRID bias adjustment factors and the FRP measured by MODIS over the same areas are shown, as are the coefficients of determination (r^2), at both 5° and hourly resolution (which is the native FRP-GRID product resolution) and also at a weekly resolution accumulated over the entire LSA SAF geographic region.

LSA SAF Region	**Abbreviation**	**Validation Results: Slope (r^2)**	
		5.0° and hourly	**weekly and regional**
northern Africa	NAfr	1.04 (0.76)	1.15 (0.96)
southern Africa	SAfr	1.02 (0.91)	1.24 (0.97)
South America	SAme	0.97 (0.34)	1.89 (0.83)
Europe	Euro	1.72 (0.19)	4.94 (0.84)

Table 4: Trace gas and particulate smoke emission factors (η) for species (s) based on extratropical forest fuels, taken from Andreae and Merlet (2001). * The emission factor for BC and OC was derived specifically for use in this study (see main text).

Species	**Emissions factor (g kg^{-1} DM)**
Black carbon (BC)	1.7*
Organic carbon (OC)	8.6-9.7
Organic matter (OM)	42*
Total particulate matter (TPM)	17.6±6.4
Fine mode aerosol (PM2.5)	13.0±7.0
Carbon Monoxide (CO)	107±37